

# INFLUENCE OF STELLAR MULTIPLICITY ON PLANET FORMATION. III. ADAPTIVE OPTICS IMAGING OF KEPLER STARS WITH GAS GIANT PLANETS

JI WANG<sup>1</sup>, DEBRA A. FISCHER<sup>1</sup>, ELLIOTT P. HORCH<sup>2</sup> AND JI-WEI XIE<sup>3</sup>,  
(Received; Accepted)  
*to appear in ApJ*

## ABSTRACT

As hundreds of gas giant planets have been discovered, we study how these planets form and evolve in different stellar environments, specifically in multiple stellar systems. In such systems, stellar companions may have a profound influence on gas giant planet formation and evolution via several dynamical effects such as truncation and perturbation. We select 84 Kepler Objects of Interest (KOIs) with gas giant planet candidates. We obtain high-angular resolution images using telescopes with adaptive optics (AO) systems. Together with the AO data, we use archival radial velocity data and dynamical analysis to constrain the presence of stellar companions. We detect 59 stellar companions around 40 KOIs for which we develop methods of testing their physical association. These methods are based on color information and galactic stellar population statistics. We find evidence of suppressive planet formation within 20 AU by comparing stellar multiplicity. The stellar multiplicity rate for planet host stars is  $0_{-0}^{+5}\%$  within 20 AU. In comparison, the stellar multiplicity rate is  $18\pm 2\%$  for the control sample, i.e., field stars in the solar neighborhood. The stellar multiplicity rate for planet host stars is  $34\pm 8\%$  for separations between 20 and 200 AU, which is higher than the control sample at  $12\pm 2\%$ . Beyond 200 AU, stellar multiplicity rates are comparable between planet host stars and the control sample. We discuss the implications of the results to gas giant planet formation and evolution.

*Subject headings:*

## 1. INTRODUCTION

Almost half of sun-like stars are members of binary or multiple star systems (hereafter MSS, Raghavan et al. 2010; Duquennoy & Mayor 1991). During the formation of a star-planet system, the presence of a companion star is likely to perturb or truncate the protoplanetary disk (e.g., Holman & Wiegert 1999; Jang-Condell 2007). These effects would affect the formation rate of planets around the stellar components of MSS. Indeed, observations of star forming regions show that protoplanetary disks around MSS have shorter lifetimes than disks around single star systems (hereafter SSS, Kraus et al. 2012). Furthermore, after planet formation, dynamical interactions with stellar companions could affect the orbital evolution of a planet and its survival rate via perturbation (Wu & Murray 2003; Naoz et al. 2012), disk-driven migration (Lin & Papaloizou 1986; Tanaka et al. 2002) and planet-planet scattering (Rasio & Ford 1996; Chatterjee et al. 2008).

Despite many theoretical and numerical studies of planets in MSS, the planet occurrence rate in MSS is still uncertain. There have been numerous estimates of the planet occurrence rate for solar-type

stars based on the Kepler results (e.g., Howard et al. 2012; Fressin et al. 2013); however, these studies do not distinguish between planet host stars in SSS or MSS. The lack of stellar multiplicity information prevents us from comparing the planet occurrence rate between SSS and MSS. The comparison would provide insights into the influence of stellar companions on planet formation. The discovery of thousands of planet candidates from the Kepler mission (Borucki et al. 2011; Batalha et al. 2013; Burke et al. 2014) provides a unique opportunity to study planets in MSS (e.g., Wang et al. 2014a)

There are two ways of studying planets in MSS. First, one can select a sample of known MSS and then search for planets around each of the component stars (the Planet-Quest approach, e.g., Konacki 2005; Eggenberger & Udry 2007; Konacki et al. 2009; Toyota et al. 2009). Unfortunately, for ground based surveys, the detection efficiency of planets in MSS is affected by flux contamination from the additional stellar components (Wright et al. 2012). Flux contamination also reduces the signal to noise ratio (SNR) of a transiting planet (Fressin et al. 2013; Wang et al. 2014a). On the other hand, the Star-Quest approach is an effective way to study planets in MSS. Using a sample of known stars with planets, it is possible to determine the fraction of MSS in that sample (e.g., Luhman & Jayawardhana 2002; Patience et al. 2002; Wang et al. 2014b; Ngo et al. 2015). From a technical standpoint, it is much easier to detect stellar companions than planetary companions, making the Star-Quest approach much eas-

Electronic address: ji.wang@yale.edu

<sup>1</sup> Department of Astronomy, Yale University, New Haven, CT 06511 USA

<sup>2</sup> Department of Physics, Southern Connecticut State University, 501 Crescent Street, New Haven, CT 06515, USA

<sup>3</sup> Department of Astronomy & Key Laboratory of Modern Astronomy and Astrophysics in Ministry of Education, Nanjing University, 210093, China

ier and more sensitive to lower mass planets. Previous observational studies have suggested that the presence of a stellar companion suppresses planet formation (e.g., Eggenberger et al. 2011). However, these studies have not fully considered biases in target selection and planet detection or the observational incompleteness in the search for stellar companions of planet host stars. Wang et al. (2014a) discuss the above concerns and find that planet formation is suppressed by stellar companions with separations up to 1500 AU.

Wang et al. (2014b,a) summarize the works following the Star-Quest approach prior to 2014. Since then, more progress has been made. These new results suggest that visual stellar companions are not rare around planet host stars. Using the Lucky Imaging technique, Lillo-Box et al. (2014) find that 32.8% of Kepler planet host stars have at least one visual stellar companion within  $6''$ . Based on adaptive optics (AO) imaging of 87 Kepler planet host stars, Dressing et al. (2014) find that 31.0% of planet host stars have stellar companions within  $4''$ . Law et al. (2014) observe 715 Kepler stars with planet candidates with the Robo-AO system. They find 7.4% of Kepler planet host stars have stellar companions within  $2.5''$ . However, the fraction of gravitationally bound companions is uncertain from these surveys. Using the speckle imaging technique, Horch et al. (2014) detect 49 stellar companions within 1 arcsec around over 600 Kepler stars with planet candidates. The majority of the detected companions are likely to be gravitationally bound to the planet host stars based on a statistical argument. Accounting for detection incompleteness, they conclude that the stellar multiplicity rate for planet host stars is similar to stars in the solar neighborhood. Gilliland et al. (2014) observe 23 Kepler stars with small and cool planet candidates using the Hubble Space Telescope. They find evidence that physically-associated stellar companions are more common around planet host stars than around field stars in the solar neighborhood. The Kepler stars in the aforementioned studies have an average Kepler magnitude of 13.5. Assuming that they are solar-type stars, the average distance is  $\sim 600$ -700 pc. More recently, Ngo et al. (2015) focus on a sample of host stars for hot Jupiters (HJs) that were discovered and confirmed by ground-based observations. They use AO imaging and conduct multiple-epoch observations to confirm physical association by measuring common proper motions of stellar components. The stellar multiplicity rate for HJ host stars is almost twice as high as that for stars in the solar neighborhood for stellar separations between 50 and 2000 AU. The overabundance of stellar companions for HJ host stars suggests the positive role of stellar companions in HJ formation and evolution.

While rapid progress has been made since 2014, there are still a number of issues for the Star-Quest approach. First, there is a selection bias against MSS for work on planets detected by ground-based observations. MSS with small separations and considerable flux contamination are usually excluded in

ground-based surveys for planets (e.g., Wright et al. 2012). The selection bias is difficult to quantify and correct, so converting the measured stellar multiplicity rate to planet occurrence rate is challenging (Wang et al. 2014a). Second, most studies focus on a single detection technique for stellar companions. The high-angular resolution imaging technique has been the dominant method. However, the physical association of stellar companions is difficult to assess for Kepler stars. This becomes an issue when calculating the stellar multiplicity rate which concerns only gravitationally bound companions. Third, the imaging techniques are not effective in detecting stellar companions within or near the diffraction limits of telescopes, which correspond to 20-50 AU in physical separation. Stellar companions at smaller separations can be more effectively detected by measuring the radial velocity (RV). So far, only a few studies following the Star-Quest approach use the RV technique in combination with the high-angular resolution imaging technique, which dramatically increases the search completeness for stellar companions (Knutson et al. 2013; Wang et al. 2014a; Ngo et al. 2015).

Finally, the control sample to be compared is not a perfect sample. Field stars in the solar neighborhood usually serve as a control sample for stars without planets, but studies on planet occurrence rate suggest that the majority of stars host at least one planet (e.g., Mayor et al. 2011; Howard et al. 2012; Fressin et al. 2013; Dressing & Charbonneau 2013). In order to construct a more meaningful control sample, we can find other stars that do not have planets down to a certain mass and up to a certain orbital separation (e.g., Eggenberger & Udry 2007), or we can continue to use the field stars as a control sample but set a planet mass/radius and separation range to limit the level of contamination of planet host stars. For example, if we consider only gas giant planets within  $\sim 1$  AU, then the stars in the solar neighborhood can serve as a reasonable control sample because fewer than 10% of stars have gas giant planets within 1 AU (Cumming et al. 2008; Mayor et al. 2011).

To address the above issues, we have conducted a search for stellar companions for 84 Kepler stars with gas giant planets within  $\sim 1$  AU. This sample of stars is not biased against MSS because the Kepler mission does not apply a selection criterion that excludes MSS (Brown et al. 2011). The typical full width at half maximum (FWHM) of images for Kepler target selection is  $2.5''$  and thus these images are ineffective at distinguishing binary stars. We use both RV data and high-angular resolution imaging data for these stars, so the search completeness is high compared to surveys employing only one technique. We assess the physical association of detected stellar companions using (1) their color information and (2) a statistical argument based on a galactic stellar population model. We can compare the stellar multiplicity rate for this sample to that for field stars in the solar neighborhood without a significant contamination of planet host stars in the control sample. After these issues are resolved, we

can study the influence of stellar companions on gas giant planet formation with the sample 84 Kepler planet host stars.

The paper is organized as follows. We describe the sample of Kepler stars with gas giant planets in §2. AO observation and data reduction for these stars are presented in §3. We also discuss the physical association of detected stellar companions in §4. We synthesize the results of different techniques in the search for stellar companions in §5. These techniques include the RV and AO imaging techniques and the dynamical analysis. The stellar multiplicity rate of Kepler stars with gas giant planets is given in §6. Discussion and summary are given in §7 and §8.

## 2. SAMPLE DESCRIPTION

From the NASA Exoplanet Archive<sup>4</sup>, we select Kepler Objects of Interest (KOIs) that satisfy the following criteria: (1), disposition of either Candidate or Confirmed; (2), stellar effective temperature (Teff) lower than 6500 K; (3) stellar surface gravity ( $\log g$ ) higher than 4.0; (4), Kepler magnitude ( $K_P$ ) brighter than 14th mag; (5), with at least one gas giant planet ( $3.8 R_{\oplus} \leq R_P \leq 22.0 R_{\oplus}$ ). In total, we select 84 KOIs with 97 gas giant planets. Stellar and orbital parameters for these KOIs are given in Table 2. The median distance of these KOIs is 580 pc. There are 27 multi-planet systems among 84 KOIs.

There are 19 KOIs with RV observations. We obtain RV data from the Kepler Community Follow-up Observation Program<sup>5</sup> (CFOP). The majority of the RV data (14 out of 19) were taken with the HIRES instrument (Vogt et al. 1994) and reported in Marcy et al. (2014). Exceptions are KOI-1 (TrES-2, O’Donovan et al. 2006), KOI-3 (HAT-P-11 b, Bakos et al. 2010), KOI-97 (Kepler-7 b, Latham et al. 2010), KOI-128 (Kepler-15 b, Endl et al. 2011), and KOI-135 (Kepler-43 b, Bonomo et al. 2012). The Modified Julian Dates (MJDs) of the first and last RV data points and the number of RV data points for each KOI are given in Table 2.

For KOIs with high-angular resolution images from CFOP, we use the images to search for stellar companions. These images were taken at different telescopes including Keck, Palomar, MMT, Lick, and WIYN. For KOIs whose high-angular resolution images are not available, we have taken AO images using the PHARO (Palomar High Angular Resolution Observer) instrument (Brandl et al. 1997; Hayward et al. 2001) at the Palomar 200-inch telescope and the NIRC2 instrument (Wizinowich et al. 2000) at the Keck II telescope. In total, we have taken AO images for 60 out of the 84 KOIs. Telescope and photometric band information is given in Table 2. The KOIs with AO images taken through this work are also indicated in Table 2.

## 3. AO OBSERVATION AND DATA REDUCTION

### 3.1. AO Imaging with PHARO at Palomar

We observed 40 KOIs in the sample with the PHARO instrument (Brandl et al. 1997; Hayward et al. 2001) at the Palomar 200-inch telescope. The observations were made between UT July 13rd and 17th in 2014 with seeing varying between 1.0'' and 2.5''. PHARO is behind the Palomar-3000 AO system, which provides a on-sky Strehl of 86% in  $K$  band (Burruss et al. 2014). The pixel scale of PHARO is 25 mas pixel<sup>-1</sup>. With a mosaic 1K  $\times$  1K detector, the field of view (FOV) is 25''  $\times$  25''. We normally obtained the first image in  $K$  band with a 5-point dither pattern, which had a throw of 2.5''. The exposure time was set such that the peak flux of the KOI is at least 10,000 ADU for each frame, which is within the linear range of the detector. If a stellar companion was detected, we observed the KOI in  $J$  and  $H$  bands.

### 3.2. AO Imaging with NIRC2 at Keck II

We observed 27 KOIs in the sample with the NIRC2 instrument (Wizinowich et al. 2000) at the Keck II telescope. The observations were made on UT July 18th and August 18th in 2014 with excellent/good seeing between 0.3'' to 0.8''. NIRC2 is a near infrared imager designed for the Keck AO system. We selected the narrow camera mode, which has a pixel scale of 10 mas pixel<sup>-1</sup>. The FOV is thus 10''  $\times$  10'' for a mosaic 1K  $\times$  1K detector. We started the observation in  $K$  band for each KOI. The exposure time setting is the same as the PHARO observation: we ensured that the peak flux is at least 10,000 ADU for each frame. We used a 3-point dither pattern with a throw of 2.5''. We avoided the lower left quadrant in the dither pattern because it has a much higher instrumental noise than other 3 quadrants on the detector. We continued observations of a KOI in  $J$  and  $H$  bands if any stellar companions were found.

### 3.3. Contrast Curve and Detections

The raw data were processed using standard techniques to replace bad pixels, flat-field, subtract thermal background, align and co-add frames. We calculated the 5- $\sigma$  detection limit as follows. We defined a series of concentric annuli centering on the star. For the concentric annuli, we calculated the median and the standard deviation of flux for pixels within these annuli. We used the value of five times the standard deviation above the median as the 5- $\sigma$  detection limit. The median contrast curve and the 1- $\sigma$  deviation of  $K$  band AO images we used in this paper are shown in Fig. 1. Also plotted are detected stellar companions as indicated by asterisks in Fig. 1. These companions are brighter than the contrast curve, so the significance of detections is at least 5  $\sigma$ . In total, 59 stellar companions were detected around 40 KOIs. Their stellar and orbital properties are summarized in Table 4.

### 3.4. Comparison to Previous Work

Among 59 stellar companions, 29 are newly detected around 22 KOIs in this study. Furthermore,

<sup>4</sup> <http://exoplanetarchive.ipac.caltech.edu>

<sup>5</sup> <https://cfop.ipac.caltech.edu>

we add observations to 8 previously known stellar companions in additional color filters. The other stellar companions that were previously reported are noted with references in Table 4. These observation campaigns were carried out using a variety of instruments at different telescopes, e.g., AIRES at MMT (Adams et al. 2012; Dressing et al. 2014), PHARO at Palomar (Adams et al. 2012), Robo-AO at Palomar (Law et al. 2014), DSSI at WIYN and Gemini (Horch et al. 2014), and AstraLux at Calar Alto (Lillo-Box et al. 2014). When compared to previous work, we miss 11 stellar companions. They are marked with an asterisk in Table 4. All but one (KOI-372,  $\Delta K = 4.0$ ) stellar companions that we miss are very faint, with a differential magnitude range between 7.2 and 8.2. Our pipeline does not identify these companions possibly because of different detection criteria. In one case (KOI-377,  $\Delta J = 6.8$ ), the stellar companion is identified in  $K$  band, but not in  $J$  band.

#### 4. PHYSICAL ASSOCIATION

For stellar companions detected by imaging techniques, we need to confirm that they are not optical doubles/multiples. Otherwise, the unassociated stellar companions will systematically increase the stellar multiplicity rate and cause misinterpretations. To test physical association, the method of obtaining multiple-epoch images and measuring common proper motion has been proven effective (Ngo et al. 2015). In our case, Kepler stars are generally  $\sim 300$ - $1000$  pc away. While future observations are scheduled, common proper motion measurements are relatively more difficult. Given only one epoch of observation, we can use color information of detected stellar companions and assess the probability of their physical association to primary stars (Lillo-Box et al. 2014; Wang et al. 2014a). Details of this approach are given in §4.1. For stellar companions with only single-band observations, color information is not available. We can assess the probability with a galactic stellar population simulation (§4.2).

##### 4.1. Physical Association Based on Color Information

We compare the distance of a KOI and its stellar companions. If their distances do not match within uncertainty, then they are likely to be optical doubles and the physical association is excluded. For the distance of a KOI, we follow the method described in Wang et al. (2014a). We calculate the distant modulus for each KOI. The  $V$  band apparent magnitude is obtained through the NASA Exoplanet Archive. The  $V$  band absolute magnitude is calculated using the Yale-Yonsei (Y2) stellar evolution model (Demarque et al. 2004). The input parameters for the Y2 model are  $T_{\text{eff}}$ ,  $\log g$ , age, and  $[\text{Fe}/\text{H}]$ , which are also obtained through the NASA Exoplanet Archive.  $V$  band extinction ( $A_V$ ) is obtained from the Mikulski Archive for Space Telescopes<sup>6</sup> (MAST). With the apparent and absolute

$V$  band magnitudes and the extinction  $A_V$ , we can calculate the distance modulus of a KOI and thus its distance. For those KOIs whose extinctions are not available, we use  $K$  band distance modulus assuming zero extinction in  $K$  band.

For stellar companions around a KOI, we use the color information, if available, to estimate their distances. We have color information, i.e., multi-band detections, for 21 companions. We convert the differential magnitudes to the true color of the companion. Based on the color information, we estimate the effective temperature of a stellar companion using Table 5 in Kraus & Hillenbrand (2007). For stellar companions detected in more than 2 bands, we use the mean effective temperatures weighted by uncertainties. Once the effective temperature is available, we can find the corresponding  $K$  band absolute magnitude for a stellar companion. Its apparent  $K$  band magnitude can be calculated from the differential  $K$  band magnitude and the apparent  $K$  band magnitude of the KOI. The  $K$  band distance modulus can be calculated assuming zero extinction. The distance modulus can then be used to estimate the distance of a stellar companion.

In the above calculation, extinctions in different bands need to be considered. Otherwise, a stellar companion would appear redder and closer. To account for extinction in different bands, we use a linear relation between  $A_\lambda/A_V$  and  $1/\lambda$  (Gordon et al. 2003). Since we are only interested in the wavelength region between  $0.55 \mu\text{m}$  ( $V$  band) and  $2.19 \mu\text{m}$  ( $K$  band), a linear relation is a reasonable approximation. On one end, we assume  $K$  band extinction to be zero. On the other end, we use the  $A_V$  from the MAST archive. Extinctions in  $r$ ,  $i$ ,  $z$ ,  $J$ , and  $H$  bands are interpolated between  $A_V$  and  $A_K$ .

The estimated distances of 21 companions are reported in Table 4. For these companions with color information, 6 have estimated distances that are  $2\text{-}\sigma$  inconsistent with the primary stars. Therefore, they are unlikely to be physically associated with the KOIs and thus are not considered in the following analyses. All 5 companions with color information and less than  $1''$  angular separations have consistent distances with their KOIs. This is consistent with the finding that stellar companions with sub-arcsec separations are mostly gravitationally bound to KOIs (Horch et al. 2014). For stellar companions with  $1.0''$  to  $3.0''$  separations, 2 out of 11 (18%) have inconsistent distances and are thus not physically associated with their KOIs.

##### 4.2. Physical Association Based on Galactic Stellar Population Model

For the stellar companions without color information, we cannot adopt the method described in §4.1. However, their physical association needs to be addressed because the frequency of optical doubles/multiples is not negligible: 6 out of 21 stellar companions with color information are not gravitationally bound. We therefore develop a statistical approach to assess the physical association of detected stellar companions.

<sup>6</sup> <http://archive.stsci.edu/>

Using the TRILEGAL galaxy model (Girardi et al. 2005), we run two sets of simulations. In the first set, we turn off binary parameters and calculate the fraction of optical doubles/multiples as a function of  $K_1$ ,  $K_2$  and  $\Delta\theta$ , where  $K_1$  is the magnitude of primary star,  $K_2$  is the magnitude of the brightest nearby star,  $\Delta\theta$  is the radius range in arcsec. In the second set of simulation, we consider both optical doubles/multiples and gravitationally bound systems. From results of both sets of simulation, we can calculate the relative contribution of optical doubles/multiples and gravitationally bound stellar systems at a given combination of  $K_1$ ,  $K_2$  and  $\Delta\theta$ , which allows us to calculate the probability of physical association in the absence of color information.

In each simulation, ten fields with a FOV of 1 square degree are simulated. These fields have different galactic latitudes so the combination of the results from the fields gives a better statistical result of the entire Kepler FOV. We consider two different filters,  $J$  and  $K$  bands because all detections in single filter are in either  $J$  or  $K$  band. The majority (29 out of 38) are in  $K$  band. The physical association probabilities of detected stellar companions in single filter are given in Table 4. We also provide a calculator for the probability of physical association as a function of  $K_1$ ,  $K_2$  and  $\Delta\theta$  in  $r$ ,  $z$ ,  $J$ ,  $H$  and  $K$  filters<sup>7</sup>.

#### 4.3. Comparing Two Physical Association Methods

We check the consistency of two methods for testing physical association. Since there are 21 stellar companions with color information, we can use this sample to perform the test: how physical association probabilities (in  $K$  band) correlate with acceptances/rejections based on color information. We divide the physical association probabilities into 3 intervals, [0.00-0.33], [0.33-0.67], and [0.67,1.00]. For the lower probability interval [0.00-0.33], 2 out of 3 stellar companions (KOI-98 and KOI-377) are rejected based on color information at 2- $\sigma$  level. For the median probability interval [0.33-0.67], 2 out of 3 stellar companions (KOI-377 and KOI-3444) are rejected based on color information. For the higher probability interval [0.67-1.00], 2 out of 15 stellar companions (KOI-97 and KOI-1812) are rejected based on color information. These results demonstrate consistency between these two methods. At a physical association probability smaller than 0.33, despite small number statistics, the majority (67%) of stellar companions are rejected based on color information. In contrast, at a physical association probability higher than 0.67, the majority of stellar companions (87%) show consistent colors to be physically associated.

## 5. SYNTHESIZING AO OBSERVATIONS WITH OTHER TECHNIQUES

While 59 stellar companions around 40 KOIs are detected via AO observations, the AO technique is not sensitive to stellar companions that are too close

to spatially resolve, nor is it sensitive to stellar companions that are too faint to detect with a sufficient SNR. By conducting simulations, we can calculate the search completeness of AO observations.

We define a parameter space,  $a - i$  space, where  $a$  is the semi-major axis of a companion star, and  $i$  is the angle between the sky plane and the companion star orbital plane. We divide the parameter space into a grid ( $\Delta a = 0.5$  AU,  $\Delta i = 10^\circ$ ). We simulate 1000 companion stars at each gridpoint in the  $a - i$  parameter space. The mass ratio distribution of simulated companions follows a Gaussian distribution from Duquennoy & Mayor (1991), i.e.,  $\bar{q} = m_2/m_1 = 0.23$ ,  $\sigma_q = 0.42$ . We use the median orbital eccentricity for binary stars ( $e = 0.4$ ) and a random true anomaly distribution in simulations. If the contrast ratio ( $\Delta$  Mag) between a simulated companion and the primary star is smaller than the value given by the 5- $\sigma$  AO contrast curve, then we record it as a detection. The median AO completeness contours are plotted in Fig. 2.

For the parameter space on the  $a - i$  plane that AO is not sensitive to, we use other observations or techniques to constrain the presence of stellar companions.

### 5.1. Radial Velocity Observation

There are 19 KOIs in our sample with at least 3 epochs of RV observation. Following the description of Wang et al. (2014a), we use the Keplerian Fitting Made Easy (KFME) package (Giguere et al. 2012) to analyze the RV data. For cases in which the number of RV data points are not adequate to constrain a Keplerian orbit, we use linear fitting to check if the RV data exhibit long-term trend. The RV data serve two purposes. First, they reveal stellar companions via RV trends. Among 19 KOIs with RV data, however, only KOI-5 exhibits a RV trend. The stellar companion that can potentially induce the trend is constrained to be beyond 7 AU (Wang et al. 2014a). More recent RV data suggest that, in addition to two transiting planet candidates, two more distant components exist in KOI-5 system (Howard Isaacson, private communication). One is a sub-stellar companion with a period of  $\sim 2700$  days and the other one is the AO-imaged stellar companion. Therefore, we consider the closest stellar companion to KOI-5 to have a projected separation of 40.3 AU (Table 4).

The second purpose the RV data serve is to constrain the presence of stellar companions in the non-detection cases. Given the RV data, we can study the completeness of searching for stellar companions by simulations (Wang et al. 2014b,a). Similar to the AO completeness study, we simulate 1000 companion stars on each grid point and count the number of simulated companion stars that can be detected given the time baseline, observation epochs, and measurement uncertainties of the RV data. The median RV completeness contours are plotted in Fig. 2.

### 5.2. Dynamical Analysis

<sup>7</sup> [http://www.astro.yale.edu/jwang/Cal\\_Prob\\_PA.py](http://www.astro.yale.edu/jwang/Cal_Prob_PA.py)

In addition to the RV and AO data, further constraints on potential stellar companions can be placed on multi-planet systems. There are 27 (32% of the sample) multi-planet systems in our sample for which we can apply a dynamical analysis (Wang et al. 2014b). This dynamical analysis makes use of the co-planarity of multi-planet systems discovered by the Kepler mission (Lissauer et al. 2011). A stellar companion with high mutual inclination to the planetary orbits would have perturbed the orbits and significantly reduced the co-planarity of planetary orbits, and hence the probability of multi-planet transits. Therefore, the fact that we have observed multiple transiting planet helps to exclude the possibility of a highly-inclined stellar companion. The dynamical analysis is complementary to the RV technique because it is sensitive to stellar companions with large mutual inclinations to the planetary orbits. The parameter space to which the dynamical analysis is sensitive is shown in Fig. 2.

### 5.3. Combining Results From Different Techniques

For the RV and AO observations, detection completeness contours are calculated based on simulations given the time baseline, cadence, measurement uncertainties, and the contrast curve. For the dynamical analysis, numerical integrations give the fraction of time when multiple planets can stay with small mutual inclinations ( $< 5^\circ$ ) so that multiple transiting planets can be observed (Wang et al. 2014b). We denote  $c_{RV}$ ,  $c_{AO}$  and  $c_{DA}$  as the completenesses at a given point in the  $a-i$  parameter space, overall completeness  $c$  is equal to  $1 - (1 - c_{RV}) \times (1 - c_{AO}) \times (1 - c_{DA})$ .

The completeness is then integrated over the  $a-i$  parameter space. For the integration, distribution functions of  $a$  and  $i$  are necessary to account for contribution at different places in  $a-i$  parameter space. The result of the integration is sensitive to the adopted distribution function. Since the distribution function of  $a$  is uncertain for planet host stars and measuring the distribution is the main goal of this paper, we adopt an iterative approach to incorporate  $a$  distribution of stellar companions. For the first iteration, we assume a log-normal distribution for  $a$  (Duquennoy & Mayor 1991; Raghavan et al. 2010). However, this distribution is not representative for stars with planets (Wang et al. 2014a), so in the subsequent iterations we adopt the  $a$  distribution from §6. The iteration stops when  $a$  distributions from two consecutive iterations differ less than 1% at any separations.

We assume a random distribution of  $-\cos i$  for systems with only one transiting planet, and the  $i$  distribution from Hale (1994) for systems with multiple transiting planets. The treatment for multiple transiting planet systems is detailed in Wang et al. (2014b), i.e., a coplanar distribution for stellar companions within 15 AU, a random  $-\cos i$  distribution for stellar companions beyond 30 AU, and a mixture of the previous two  $i$  distributions for intermediate separations between 15 and 30 AU.

### 5.4. Correcting For Detection Bias Against Planets in Multiple-Star Systems

Planets in MSS are more difficult to find using the transit method because of flux contamination. The effect of this bias and a correction method have been discussed in Wang et al. (2014a). We briefly introduce the method here.

We conduct simulations to quantify the detection bias against planets in MSS. For each KOI, we choose the one planet that gives the highest SNR. We add a companion star in the system and calculate the SNR in the presence of flux contamination for two cases: planet transiting the primary star and planet transiting the secondary star. If the SNR is higher than 7.1 (Jenkins et al. 2010), then the planet can still be detected, but with a lower significance. We randomly assign a stellar companion (secondary star) to a KOI (primary star) and repeat this procedure 1000 times for both the primary and the secondary star. We record the fraction of planet detections in 2000 simulations considering flux contamination. We designate the fraction to be  $\alpha$ , which will be used in correcting for the bias of detecting planets in MSS. For example,  $\alpha = 0.95$  indicates that 95% of planets would still be detected in the presence of flux contamination. In order to account for the 5% missed planets, for every  $N$  MSS that host such a planet, we should use  $N/\alpha$  to represent the underlying MSS population that host such a planet. Since the transiting signal of gas giant planets is large, they are rarely missed in Kepler observations. Therefore,  $\alpha$  is close to one in most cases.

## 6. STELLAR MULTIPLICITY RATE FOR KEPLER STARS WITH GAS GIANT PLANETS

The Kepler mission has provided us with a large sample of planet candidates. However, we do not know *a priori* whether a given planet host star is in SSS or MSS. Follow-up observations are critical in identifying additional stellar companions in planetary systems. Even in the case of non-detection with RV and AO, we can calculate the probability of a star being in a MSS based on the completeness study (§5.3). For example, given the overall completeness  $c$  and the stellar multiplicity rate (MR), the probability of the star having an undetected companion (or being in a MSS) within  $r$  (in AU) is:

$$p_M(a \leq r) = \int_{a \leq r} \text{MR}(a) \int (1 - c(a, i)) \omega(i) di da, \quad (1)$$

where  $\omega(i)$  is a weighting function for  $i$ . For single planetary systems,  $\omega(i)di = d(-\cos i)$ . For multiple planetary systems,  $\omega(i)di$  is a piecewise function depending on stellar separation  $a$  (§5.3). The form of the weighting function for  $a$ ,  $\text{MR}(a)$ , was also discussed in §5.3.  $\text{MR}(a)$  is the  $a$  distribution of stellar companions for planet host stars. Here, we use  $\text{MR}(a)$  as a differential distribution, which is the derivative of a cumulative distribution  $\text{MR}(a \leq r)$ , i.e., Equation 3, where both  $a$  and  $r$  are semi-major axis of an orbit.  $\text{MR}(a)$  and  $\text{MR}(a \leq r)$  are de-

rived in an iterative way. For each iteration, we use  $MR(a)$  from the previous iteration in Equation 1 to calculate  $p_M$ , which is then fed into Equation 2 and 3 to calculate  $MR(a)$  in the new iteration. The iteration converges until  $MR(a)$  from the new iteration and  $MR(a)$  from the previous iteration agree within 1% at any separations. Following this procedure, we calculate the number of MSS,  $N_M$ , and the number of SSS,  $N_S$ . Since  $N_M$  and  $N_S$  are the sums of probabilities, they are not necessarily integers:

$$N_M(a \leq r) = \sum_{k=1}^N [p_M(a \leq r, k) / \alpha(k)], \quad N_S(a \leq r) = \sum_{k=1}^N [1 - p_M(a \leq r, k)], \quad (2)$$

where  $N$  is the total number of stars in the sample,  $p_M(k)$  is the probability of the  $k_{\text{th}}$  star being in a MSS,  $\alpha(k)$  is the correction factor for the detection bias for planets in MSS (discussed in §5.4). Note that there is an implicit correction factor for SSS in Equation 2, but that this factor is 1. If a physically associated stellar companion is detected within a semi-major axis  $r$  to a KOI, then  $p_M(a \leq r)$  is assigned to 1. We note that AO observation only measures projected separation. The conversion from projected separation to semi-major axis is addressed by a Monte-Carlo simulation assuming that stellar companions have randomly oriented orbits (§6.1). We also assign  $\alpha$  to 1 because no bias exists in this case since a planet has already been detected in a MSS. The cumulative stellar multiplicity rate for planet host stars can be calculated:

$$MR(a \leq r) = \frac{N_M(a \leq r)}{N_M(a \leq r) + N_S(a \leq r)}. \quad (3)$$

### 6.1. Considering Physical Association Probability and Companion Orbital Orientation

Not all AO detected stellar companions are physically associated with the KOI. Therefore, we need to consider the probability of physical association when calculating  $N_M$ , which is later used for the cumulative stellar multiplicity rate calculation (Equation 3). Similarly,  $N_M$  may be different due to the orbit orientation of detected stellar companions. AO observation only measures projected separation, but we need semi-major axis in  $N_M$  calculation. Since orbital orientation, eccentricity and true anomaly are required to convert projected separation to semi-major axis, and these are not known for a single epoch AO observation, the conversion cannot be performed on an individual system. However, we can run a Monte-Carlo simulation to calculate  $N_M$  and its uncertainty due to physical association probability and companion orbital orientation.

We developed two methods to calculate the probability of physical association in §4.1 and §4.2. For detections in multiple filters, we estimate the distance of a stellar companion based on its color information. We exclude stellar companions whose distances are inconsistent with the KOI distance at more than  $2\text{-}\sigma$  level. For detections in only one filter, we estimate the probability of physical association using a galactic stellar population model .

Then a random number following the uniform distribution between 0 and 1 is generated. If the random number is higher than the physical association probability, then the detection is excluded in the stellar multiplicity rate calculation. To account for the uncertainty in converting projected separation to semi-major axis, we assume randomly-orientated companion orbits. We use the median orbital eccentricity for companion stars ( $e = 0.4$ ) and a random true anomaly distribution in simulations. The calculation for  $N_M$ ,  $N_S$ , and the stellar multiplicity rate is repeated for 1000 times for their values and uncertainties.

### 6.2. Treatments For Different Stellar Separations

For small separations, i.e.,  $a \leq 10$  AU, the RV data provide an effective constraint on stellar companions. As shown in Fig. 2, the completeness of the RV technique is higher than 50% for the majority of parameter space within 10 AU. However, RV data are available for only 19 out of 84 KOIs. While considering all KOIs for stellar multiplicity rate within 10 AU seems to improve statistics, it in fact does not help because the majority of KOIs do not have data to constrain stellar companions within 10 AU. Instead, these KOIs without RV data outnumber KOIs with RV data and thus dominate the statistics. Since we use statistics of field stars in the solar neighborhood as an initial guess for stellar separation distribution for stellar companions (see §5.3), the lack of RV data for the majority of the KOI sample results in the lack of constraint for stellar companions within 10 AU. Therefore, the resulting stellar separation distribution for these 84 KOIs would be similar to that of field stars in the solar neighborhood. The similarity of stellar separation distribution is not physical but rather a result of a lack of constraint from RV data for the majority of the sample.

To avoid the above problem, we consider only KOIs with RV data when calculating stellar multiplicity rate for small separations. To define small separations, we choose separations at which the completeness of AO data becomes higher than the completeness of RV data. Based on Fig. 2, the transition separation is at 30-60 AU, so we adopt 50 AU as the transition separation. For stellar multiplicity rate within 50 AU, we consider 19 KOIs with both RV and AO data. For stellar multiplicity rate beyond 50 AU, we consider all 84 KOIs for which we have AO data.

One concern of using KOIs with RV data is the selection bias of RV observation and its potential influence on stellar multiplicity rate measurement. If RV observations are preferentially conducted for single stars or stars without significant flux contamination, then the stellar multiplicity rate for these KOIs would be lower because of selection bias. However, we have discussed this issue in Section 4.5 of Wang et al. (2014a) showing no evidence of such selection bias. For this work, we also checked the 84 Kepler stars in our sample. For 19 stars that received RV follow-up observations, 5 have stellar companions within  $2''$ , one has severe flux contam-

ination, i.e., delta mag smaller than 2 mag. For 65 stars without RV data, 11 have stellar companions within  $2''$ , 4 have severe flux contamination. The detection rates of stellar companions are comparable between stars receiving RV observations and stars without RV observations. Therefore, there is no evidence of selection bias of RV follow-up observations, i.e., stars with RV data tend to have fewer stellar companions or fewer bright companions than stars without RV data.

### 6.3. *Stellar Multiplicity Rate vs. Stellar Companion Separation*

Fig. 3 shows the comparison between the cumulative stellar multiplicity rate for field stars (blue hatched region, Duquennoy & Mayor 1991; Raghavan et al. 2010) and that for planet host stars (red hatched regions). The field stars serve as a control sample for comparison. Hatched regions represents  $1\text{-}\sigma$  uncertainties. For field stars in the solar neighborhood, we adopt a 2% uncertainty (Raghavan et al. 2010). For planet host stars, we consider two sources of uncertainty. First, we consider the uncertainty induced by physical association (§6.1). Second, we consider Poisson noise by propagating the uncertainty in Equation 3. The two uncertainties are summed in quadrature for the final uncertainty.

The stellar multiplicity rate for planet host stars is consistent with zero and stays flat at  $0_{-0}^{+5}\%$  for stellar separations smaller than 20 AU. For  $20 \text{ AU} < a < 200 \text{ AU}$ , the stellar multiplicity rate is  $34\% \pm 8\%$ . The increase of the cumulative stellar multiplicity rate from [0-20] AU to [20-200] AU is much faster than the control sample whose cumulative stellar multiplicity rate changes from 18% to 30%. Beyond 200 AU, the stellar multiplicity rate for planet host stars is higher than that for the control sample, but they are consistent within measurement uncertainty. The slopes for the cumulative stellar multiplicity rate change are similar between planet host stars and the control sample.

## 7. DISCUSSION

### 7.1. *Interpretation of the Stellar Multiplicity of Stars With Gas Giant Planets*

According to Fig. 3, there may be three stellar separation ranges in which stellar companions affect gas giant formation and evolution differently. For stellar separations smaller than 20 AU, planet formation is suppressed. No stellar companion has been found within 20 AU for Kepler stars with gas giant planets. This leads to a zero stellar multiplicity ( $0_{-0}^{+5}\%$ ) that is significantly lower than that for the control sample ( $18\% \pm 2\%$ ).

For separations between 20 AU and 200 AU, we notice a drastic increase of the cumulative stellar multiplicity rate for planet host stars. In contrast to the stellar multiplicity rate of  $12\% \pm 2\%$  in this separation range for the control sample, the stellar multiplicity rate is  $34\% \pm 8\%$  for planet host stars. The higher stellar multiplicity rate for planet host stars suggests that stellar companions in this sep-

aration range play an important role in gas giant planet migration, e.g., via the Lidov-Kozai mechanism. Therefore, for  $20 \text{ AU} < a < 200 \text{ AU}$ , the role of stellar companions in planet migration is more important than their role in suppressing planet formation. However, there may be a caveat asserting the role of stellar companions in planet migration. The search completeness is  $\sim 30\text{-}50\%$  between 20 and 200 AU (Fig. 2), which is the lowest in the  $a - i$  parameter space. Therefore, the stellar multiplicity rate in this separation range is the most uncertain.

For separation beyond 200 AU, the stellar multiplicity rate for planet host stars is comparable to that for the control sample, which indicates that gas giant planet formation and evolution is not significantly affected by a stellar companion.

### 7.2. *Comparison to Stars with Small Planets*

Wang et al. (2014a) measured the cumulative stellar multiplicity rate for a sample of planet host stars. This sample is dominated by stars with smaller planets, 43 out of 56 stars have only transiting planets that are smaller than  $3.8 R_{\oplus}$ . We compare the stellar multiplicity rates from Wang et al. (2014a) and this work, which focuses on gas giant planet host stars. While they are qualitatively identical, the characteristic separations are different. For example, the stellar multiplicity rate for small planet host stars intersects with control sample at  $\sim 1500 \text{ AU}$  whereas the intersection takes place at  $\sim 100 \text{ AU}$  for gas giant planets. The effective range of a stellar companion is an order of magnitude larger for small planets than for large planets: smaller planets are more prone to the influence of a stellar companion.

There may be several explanations. First, in a multi-planet system, the timescale for pericenter precession and nodal precession increases with decreasing planet mass (Takeda et al. 2008). For planet systems of the same orbital configurations, the Kozai timescale is more likely to be shorter than the timescale for pericenter precession and nodal precession for smaller planets, which makes these systems dominated by the Kozai effect due to the stellar companion. Therefore, smaller planets are more prone to the influence of a distant stellar companion because of a weaker planet-planet dynamical coupling. Second, for planet systems with both small and large planets, dynamical interaction between these two types of planets tend to eject more small planets than large planets (Xie et al. 2015 in prep.). In the presence of stellar companions, the dynamical interaction becomes more frequent and thus leads to higher loss of small planets.

### 7.3. *Correlation Between Stellar Companion Properties and Planet Properties*

Planet formation is subject to the influence of stellar companions. Therefore, planets with different properties (e.g., orbital period and planet radius) may be a result of different properties of stellar companions. Here, we study whether the difference of

stellar companions results in the difference of planet properties.

For properties of stellar companions, we focus on their differential magnitudes ( $\Delta \text{Mag}$ ). Since the majority (51 out of 59) of detected stellar companions have differential magnitudes in  $K$  band, we use the differential magnitudes in  $K$  band. For those whose  $K$  band differential magnitudes are not available, we do not use them in the following analysis.

To find evidence that stellar companion properties affect planet properties, we adopt a K-S-test-based method that has been used to search for different populations divided by a parameter (Quinn et al. 2014; Buchhave et al. 2014). The method is described as follows. We choose a value  $x$  for a planet property parameter. The value divides the sample into two sub-samples. We then compare the stellar companion properties of two sub-samples with the K-S test. The  $p$  value of the K-S test is recorded. By varying  $x$  and repeating the K-S test, we obtain a function  $p(x)$ . If there are certain  $x$  values that result in significant difference between two sub-samples, these values may represent characteristic values that divide different planet populations. These populations are a result of different properties of stellar companions. Because not all stellar companions are physically associated, we need to account for the effect of inclusion of optical double/multiples. The uncertainty due to this effect is addressed in a Monto Carlo simulation. In each trial, we draw a subset of detected stellar companions based on the probability of their physical association. We apply the K-S-test-based method to the subset and record  $p(x)$ . We repeat the process for 1000 times and find the median and confidence intervals at different levels.

Fig. 4 shows the  $p$  value in K-S test as a function of planet orbital period. The K-S test compares the  $\Delta \text{Mag}$  of two sub-samples divided by orbital period. The K-S test-based method suggests that there may be three different populations of gas giant planets. We caution that this finding is not conclusive at this stage given small number statistics. If using  $p=0.05$  as a threshold, the dividing orbital periods are  $\sim 10$  and  $\sim 70$  days. The  $p$ -value dip at  $P \sim 10$  day is broad extending from 7 to 22 days. Hereafter we use  $P \sim 10$  days as a representative value. The stellar properties of these three populations may be distinctively different. Fig. 5 shows the  $\Delta \text{Mag}$  distribution. Stars with gas giant planets with  $P < 10$  days tend to have more stellar companions with small differential magnitudes ( $\Delta \text{Mag} < 2$ ). In comparison,  $\Delta \text{Mag}$  for stars with gas giant planets with  $P \geq 70$  days tend to be fainter but peak at  $\Delta \text{Mag} \sim 3$ . However, the peak may be due to a lack of sensitivity for fainter stellar companions. The  $\Delta \text{Mag}$  for Stars with gas giant planets with  $10 \leq P < 70$  days lies in between the previous two populations.

We check whether the finding of three distinct populations is prone to inclusion of false positives. One major cause of false positive is underestimation of radius due to flux contamination. Horch et al. (2014) estimate the effect as a function of  $\Delta \text{Mag}$

in Kepler band in two scenarios: object transiting primary star and secondary star. After applying their calculation, there are five KOIs that could be false positives. All the potential false positives are for the scenarios in which an object is transiting secondary star. These KOIs are KOI-17, KOI-375, KOI-633, KOI-2672, and KOI-3678. Among them, KOI-17, also known as Kepler-6, has been confirmed (Dunham et al. 2010). KOI-2672 is a system with multiple transiting planet candidates, so the false positive probability is low (Lissauer et al. 2012). The stellar companions for KOI-375, KOI-633, and KOI-3678 are only detected in  $K$  band and have differential magnitudes of 3.3, 3.9 and 3.3 mag. If physically associated, the  $K$  band differential magnitudes would put the stellar companions in the range of early-type M dwarfs. Such low-mass stars are less likely to harbor gas giant planets, which makes the scenario in which an object transits the secondary star less probable. Given the false positive rate of  $\sim 20\%$  (Fressin et al. 2013), there would be at most one KOI that is a false positive, which will not significantly reduce the peak seen in Fig. 5. However, we must caution again that the three-population hypothesis is preliminary and remains to stand the test of more observations and a larger sample.

#### 7.4. Comparison to Other Results

The stellar multiplicity rate of planet host stars has been a research interest for a number of works (see §1 for references). All previous results concerning the Kepler sample were for small planet host stars. This is because Kepler discoveries are dominated by small planets and these planets are of great interest for potential habitable worlds. Ngo et al. (2015) used a sample of stars with gas giant planets that were discovered by ground-based RV and transiting surveys. In their ‘‘Friends of Hot Jupiters’’ project, they found that the stellar multiplicity for 50 stars with hot Jupiters (HJs) is  $48 \pm 9\%$  for the stellar separation range of 50-2000 AU. We have 28 HJs in our sample, the stellar multiplicity rate we find for these separations is  $25 \pm 20\%$ . However, if considering separations smaller than 50 AU, the stellar multiplicity rate within 2000 AU is  $51 \pm 13\%$ . The significant difference is due to the drastic change of stellar multiplicity rate between 20 and 200 AU (Fig. 3).

In §7.3, we suggest that the stellar companions around HJ host stars are on average brighter than stellar companions around stars hosting longer-period gas giant planets (Fig. 5). In our sample, all stellar companions around HJ host stars have  $K$  band differential magnitudes smaller than 2.5 with one exception of KOI-17 ( $\Delta \text{Mag} = 3.8$  mag). The trend is absent in Ngo et al. (2015). None of their detected stellar companions have differential magnitudes smaller than 2.5 mag. One explanation is that they focus on stars with HJs discovered by ground-based RV and transiting surveys. In these surveys, a strong bias against MSS exists in the target selection and follow-up observations. The fact that Ngo et al. (2015) detected

many fainter stellar companions suggests that there may be a missing population of HJ systems in equal-mass binary systems. Recent discovery of HJs in WASP-94 AB system is one example of such systems (Neveu-VanMalle et al. 2014).

Law et al. (2014) observed 715 KOIs using the Robo-AO system, they found that stars hosting short-period ( $P \leq 15$  days) giant planets are 2-3 times more likely to have stellar companions than their longer-period counterparts. For our sample, we have 32 giant planets with period shorter than 15 days. When comparing the stellar multiplicity rate for stars hosting short-period planets and the rest of our sample, we do not find a significant difference. In fact, the stellar multiplicity rates for the stars with short-period planets, stars with planets with  $P > 15$  days, and the entire sample are all  $\sim 50\%$  within 5000 AU. For stars with short-period planets, they tend to have brighter stellar companions, which are easier for Robo-AO to detect. For stars with planets with longer periods, their stellar companions tend to be fainter with differential magnitudes peaking at  $\Delta \text{Mag} = 3.0$  in  $K$  band. These faint stellar companions are 1-2 mag fainter in the visible bands at which Robo-AO operates. Thus they are likely to be missed by Robo-AO given the detection limits are  $\sim 4-5$  mag in  $r$  and  $i$  band for the median performance. The portion of fainter stellar companions missing in the Robo-AO survey may explain their finding that stars hosting short-period ( $P \leq 15$  days) giant planets are 2-3 times more likely to have stellar companions. Therefore, we suspect that the finding in Law et al. (2014) may be caused by a lack of sensitivity to faint stellar companions.

Jang-Condell (2015) quantified planet formation efficiency in close binaries. The paper gave an empirical equation of gas giant planet formation efficiency as a function of primary star mass, mass ratio, binary separation and binary orbital eccentricity. Our finding of a suppressive planet formation within 20 AU is consistent with the conclusion in Jang-Condell (2015). However, Jang-Condell (2015) predicted that gas giant planets in close binaries with separations smaller than 20 AU are not entirely impossible. In comparison, there is no such planetary system in our sample. The closest stellar companion we have detected is at 40.3 AU projected separation. There are several other planetary systems in close binaries detected by the RV technique, such as  $\gamma$  Cep and HD 41004, but none of them has a binary separation smaller than 20 AU. The contrast between observations and theoretical predictions implies that a close stellar companion not only decreases the planet formation efficiency but also negatively influences planet evolution. Jang-Condell (2015) also discussed the effect of mass ratio on planet formation. While we found the tentative correlation between hot Jupiter occurrence and equal-brightness stellar companion, it is difficult to make a direct comparison because Jang-Condell (2015) focused on stellar companions with separations smaller than 100 AU whereas all but one companions in our study have separations

larger than 100 AU.

## 8. SUMMARY

We select a sample 84 KOIs with 97 gas giant planets to study the influence of stellar companions on planet formation. We obtain AO images for 60 KOIs with two instruments: PHARO at Palomar 200-inch telescope and NIRC2 at Keck II telescope. For the rest of the sample, we use AO images available from the CFOP database. In total, we have detected 59 stellar companions around 40 KOIs.

Since some of the detected stellar companions are not physically associated with the KOIs, we develop two methods of testing the physical association. The first method makes use of the color information. For stellar companions with detections in multiple filters, we estimate their masses and absolute magnitudes based on their colors. Their distances can be estimated from the absolute magnitudes, apparent magnitudes, and extinctions. By comparing the distances of stellar companions and the KOIs, we can test their physical association. The second method is based on the statistics of galactic stellar population. For stellar companions that are detected in only one filter, the color information is missing. Instead, we run galactic stellar population model to simulate the Kepler field. With the results, we estimate the relative probability of a gravitationally bound stellar companions and optical doubles/multiples. Then we can calculate the probability of physical association as a function of angular separation and differential magnitude of a stellar companion. With these two methods of testing physical association, we can effectively exclude the effect of foreground and background stars on stellar multiplicity rate.

We find that the stellar multiplicity rate for planet host stars is  $0_{-0}^{+5\%}$  within 20 AU. In comparison, the stellar multiplicity rate is  $18\% \pm 2\%$  for the control sample, i.e., field stars in the solar neighborhood. The deficiency of stellar companions for planet host stars indicates that gas giant planet formation is suppressed by stellar companions within 20 AU. The stellar multiplicity rate for planet host star is  $34\% \pm 8\%$  for separations between 20 and 200 AU, which is higher than the control sample at  $12\% \pm 2\%$ . This suggests that stellar companions in this separation range play a important role in gas giant planet migration. Beyond 200 AU, stellar multiplicity rates are comparable between planet host stars and the control sample.

We explore whether stellar companions of different properties lead to different planet properties. We find evidence of three distinct populations of gas giant planets. They are separated by two characteristic orbital periods, 10 and 70 days. The stellar companions around stars with each planet population have different differential magnitude distributions. For example, stars with HJs ( $P < 10$  days) tend to have bright stellar companions with  $K$  band differential magnitudes smaller than 2 mag. Stars with gas giant planets with  $P \geq 70$  days tend to have stellar companions whose differential magnitudes peak at  $\sim 3.0$  mag in  $K$  band, which cor-

respond to early type M dwarf companions. We emphasize that the three-population hypothesis is still tentative, and more follow-up observations are needed to either support or disprove it.

If the three-population hypothesis survives future tests, it may have significant implications on gas giant planet formation and evolution. First, the migration of gas giant planets may be dependent upon the mass of a stellar companion. The majority of gas giant planets in our sample cannot form in situ because of a lack of building and accreting materials. They must migrate in via some mechanisms. The migration mechanisms could be the same for different planet populations, e.g., the Lidov-Kozai mechanism. Or the migration mechanisms could be different, e.g., the Lidov-Kozai mechanism for HJs and in-disk migration for longer-period planets. In either case, the migration mechanisms have to be consistent with the observed mass-dependency of stellar companions.

Second, if HJs tend to be preferentially found in binary star systems with similar magnitudes, this population of HJs have been neglected because of the concern of flux contamination. The HJs in WASP-94 AB (Neveu-VanMalle et al. 2014) and Kepler-13 AB (Szabó et al. 2011; Mazeh et al. 2012; Shporer et al. 2014; Johnson et al. 2014) systems may be the tip of iceberg for this population. Surveys that do not bias against MSS can constrain the HJ occurrence rate in binary star systems with similar magnitudes. Current and future space missions for transiting planets, e.g., the K2 mission (Howell et al. 2014) and the TESS mission (Ricker et al. 2014), may serve the purpose. In fact, the transiting signal of HJs in binary stars may already exist in ground-based transiting surveys. In

addition, AO-fed spectrographs will play an important role in validating or confirming HJs in binary stars (e.g., Crepp 2014).

*Acknowledgements* The authors would like to thank the anonymous referee whose comments and suggestions greatly improve the paper. We are grateful to telescope operators and supporting astronomers at the Palomar Observatory and the Keck Observatory. Some of the data presented herein were obtained at the W.M. Keck Observatory, which is operated as a scientific partnership among the California Institute of Technology, the University of California and the National Aeronautics and Space Administration. The Observatory was made possible by the generous financial support of the W.M. Keck Foundation. The research is made possible by the data from the Kepler Community Follow-up Observing Program (CFOP). The authors acknowledge all the CFOP users who uploaded the AO and RV data used in the paper. This research has made use of the NASA Exoplanet Archive, which is operated by the California Institute of Technology, under contract with the National Aeronautics and Space Administration under the Exoplanet Exploration Program. J.W.X. acknowledges support from the National Natural Science Foundation of China (Grant No. 11333002 and 11403012), the Key Development Program of Basic Research of China (973 program, Grant No. 2013CB834900) and the Foundation for the Author of National Excellent Doctoral Dissertation (FANEDD) of PR China. J.W. acknowledges the travel fund from the Key Laboratory of Modern Astronomy and Astrophysics (Nanjing University). We thank Eric Ford for insightful comments on interpreting the stellar multiplicity rate of planet host stars.

#### REFERENCES

- Adams, E. R., Ciardi, D. R., Dupree, A. K., Gautier, III, T. N., Kulesa, C., & McCarthy, D. 2012, *AJ*, 144, 42
- Bakos, G. Á., et al. 2010, *ApJ*, 710, 1724
- Batalha, N. M., et al. 2013, *ApJS*, 204, 24
- Bonomo, A. S., et al. 2012, *A&A*, 538, A96
- Borucki, W. J., et al. 2011, *ApJ*, 736, 19
- Brandl, B., Hayward, T. L., Houck, J. R., Gull, G. E., Pirger, B., & Schoenwald, J. 1997, in *Society of Photo-Optical Instrumentation Engineers (SPIE) Conference Series*, Vol. 3126, *Adaptive Optics and Applications*, ed. R. K. Tyson & R. Q. Fugate, 515
- Brown, T. M., Latham, D. W., Everett, M. E., & Esquerdo, G. A. 2011, *AJ*, 142, 112
- Buchhave, L. A., et al. 2014, *Nature*, 509, 593
- Burke, C. J., et al. 2014, *ApJS*, 210, 19
- Burruss, R. S., et al. 2014, in *Presented at the Society of Photo-Optical Instrumentation Engineers (SPIE) Conference*, Vol. 9148, *Society of Photo-Optical Instrumentation Engineers (SPIE) Conference Series*
- Chatterjee, S., Ford, E. B., Matsumura, S., & Rasio, F. A. 2008, *ApJ*, 686, 580
- Crepp, J. R. 2014, *ArXiv e-prints*
- Cumming, A., Butler, R. P., Marcy, G. W., Vogt, S. S., Wright, J. T., & Fischer, D. A. 2008, *PASP*, 120, 531
- Demarque, P., Woo, J.-H., Kim, Y.-C., & Yi, S. K. 2004, *ApJS*, 155, 667
- Dressing, C. D., Adams, E. R., Dupree, A. K., Kulesa, C., & McCarthy, D. 2014, *AJ*, 148, 78
- Dressing, C. D., & Charbonneau, D. 2013, *ApJ*, 767, 95
- Dunham, E. W., et al. 2010, *ApJ*, 713, L136
- Duquennoy, A., & Mayor, M. 1991, *A&A*, 248, 485
- Eggenberger, A., & Udry, S. 2007, *ArXiv e-prints*
- Eggenberger, A., Udry, S., Chauvin, G., Forveille, T., Beuzit, J.-L., Lagrange, A.-M., & Mayor, M. 2011, in *IAU Symposium*, Vol. 276, *IAU Symposium*, ed. A. Sozzetti, M. G. Lattanzi, & A. P. Boss, 409–410
- Endl, M., et al. 2011, *ApJS*, 197, 13
- Fressin, F., et al. 2013, *ApJ*, 766, 81
- Giguere, M. J., et al. 2012, *ApJ*, 744, 4
- Gilliland, R. L., Star, K. M., Adams, E. R., Ciardi, D. R., Kalas, P., & Wright, J. T. 2014, *ArXiv e-prints*
- Girardi, L., Groenewegen, M. A. T., Hatziminaoglou, E., & da Costa, L. 2005, *A&A*, 436, 895
- Gordon, K. D., Clayton, G. C., Misselt, K. A., Landolt, A. U., & Wolff, M. J. 2003, *ApJ*, 594, 279
- Hale, A. 1994, *AJ*, 107, 306
- Hayward, T. L., Brandl, B., Pirger, B., Blacken, C., Gull, G. E., Schoenwald, J., & Houck, J. R. 2001, *PASP*, 113, 105
- Holman, M. J., & Wiegert, P. A. 1999, *AJ*, 117, 621
- Horch, E. P., Howell, S. B., Everett, M. E., & Ciardi, D. R. 2014, *ApJ*, 795, 60
- Howard, A. W., et al. 2012, *ApJS*, 201, 15
- Howell, S. B., et al. 2014, *PASP*, 126, 398
- Jang-Condell, H. 2007, *ApJ*, 654, 641
- . 2015, *ApJ*, 799, 147
- Jenkins, J. M., et al. 2010, *ApJ*, 713, L87
- Johnson, M. C., Cochran, W. D., Albrecht, S., Dodson-Robinson, S. E., Winn, J. N., & Gullikson, K. 2014, *ApJ*, 790, 30

- Knutson, H. A., et al. 2013, ArXiv e-prints  
 Konacki, M. 2005, ApJ, 626, 431  
 Konacki, M., Muterspaugh, M. W., Kulkarni, S. R., & Helminiak, K. G. 2009, ApJ, 704, 513  
 Kraus, A. L., & Hillenbrand, L. A. 2007, AJ, 134, 2340  
 Kraus, A. L., Ireland, M. J., Hillenbrand, L. A., & Martinache, F. 2012, ApJ, 745, 19  
 Latham, D. W., et al. 2010, ApJ, 713, L140  
 Law, N. M., et al. 2014, ApJ, 791, 35  
 Lillo-Box, J., Barrado, D., & Bouy, H. 2014, A&A, 566, A103  
 Lin, D. N. C., & Papaloizou, J. 1986, ApJ, 309, 846  
 Lissauer, J. J., et al. 2011, ApJS, 197, 8  
 —. 2012, ApJ, 750, 112  
 Luhman, K. L., & Jayawardhana, R. 2002, ApJ, 566, 1132  
 Marcy, G. W., et al. 2014, ApJS, 210, 20  
 Mayor, M., et al. 2011, ArXiv e-prints  
 Mazeh, T., Nachmani, G., Sokol, G., Faigler, S., & Zucker, S. 2012, A&A, 541, A56  
 Naoz, S., Farr, W. M., & Rasio, F. A. 2012, ApJ, 754, L36  
 Neveu-VanMalle, M., et al. 2014, A&A, 572, A49  
 Ngo, H., et al. 2015, ArXiv e-prints  
 O'Donovan, F. T., et al. 2006, ApJ, 651, L61  
 Patience, J., et al. 2002, ApJ, 581, 654  
 Quinn, S. N., et al. 2014, ApJ, 787, 27  
 Raghavan, D., et al. 2010, ApJS, 190, 1  
 Rasio, F. A., & Ford, E. B. 1996, Science, 274, 954  
 Ricker, G. R., et al. 2014, in Society of Photo-Optical Instrumentation Engineers (SPIE) Conference Series, Vol. 9143, Society of Photo-Optical Instrumentation Engineers (SPIE) Conference Series, 20  
 Shporer, A., et al. 2014, ApJ, 788, 92  
 Szabó, G. M., et al. 2011, ApJ, 736, L4  
 Takeda, G., Kita, R., & Rasio, F. A. 2008, ApJ, 683, 1063  
 Tanaka, H., Takeuchi, T., & Ward, W. R. 2002, ApJ, 565, 1257  
 Toyota, E., et al. 2009, PASJ, 61, 19  
 Vogt, S. S., et al. 1994, in Society of Photo-Optical Instrumentation Engineers (SPIE) Conference Series, Vol. 2198, Society of Photo-Optical Instrumentation Engineers (SPIE) Conference Series, 362+  
 Wang, J., Fischer, D. A., Xie, J.-W., & Ciardi, D. R. 2014a, ApJ, 791, 111  
 Wang, J., Xie, J.-W., Barclay, T., & Fischer, D. A. 2014b, ApJ, 783, 4  
 Wizinowich, P. L., Acton, D. S., Lai, O., Gathright, J., Lupton, W., & Stomski, P. J. 2000, in Society of Photo-Optical Instrumentation Engineers (SPIE) Conference Series, Vol. 4007, Society of Photo-Optical Instrumentation Engineers (SPIE) Conference Series, ed. P. L. Wizinowich, 2–13  
 Wright, J. T., Marcy, G. W., Howard, A. W., Johnson, J. A., Morton, T. D., & Fischer, D. A. 2012, ApJ, 753, 160  
 Wu, Y., & Murray, N. 2003, ApJ, 589, 605

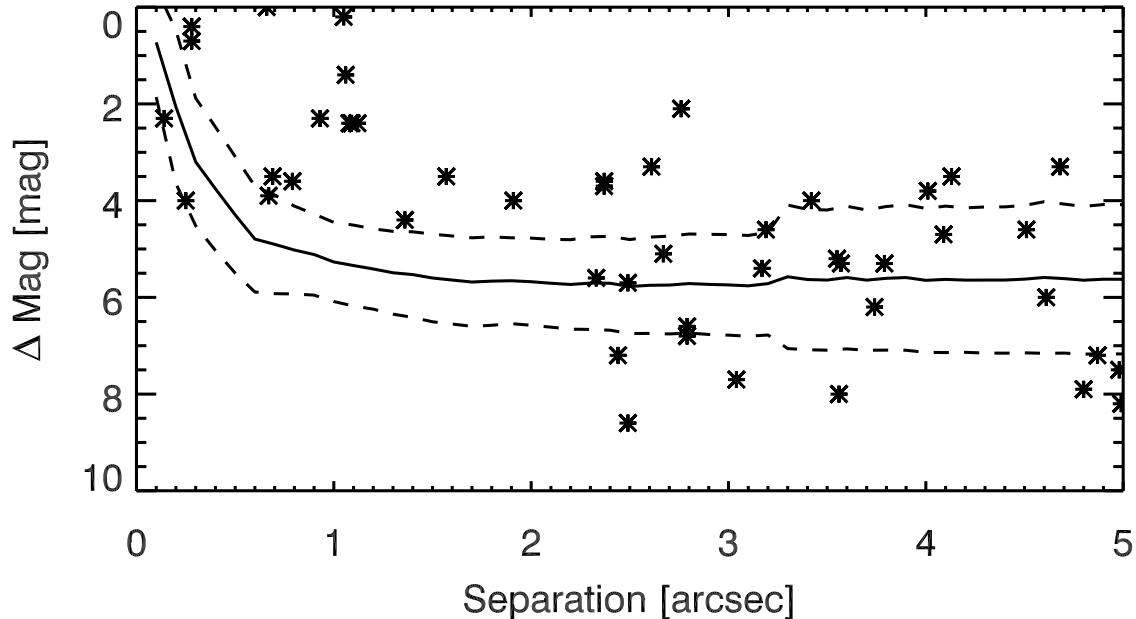


FIG. 1.— The median  $5\text{-}\sigma$  contrast curve for AO images of 84 KOIs is shown in solid line. Dashed lines are  $1\text{-}\sigma$  deviation of the contrast curve. Detections within  $5''$  are shown as asterisks. When analyzing the detection completeness, each KOI is treated individually for the observation band in which the AO image was taken. A total of 59 visual companions around 40 KOIs are detected (Table 4).

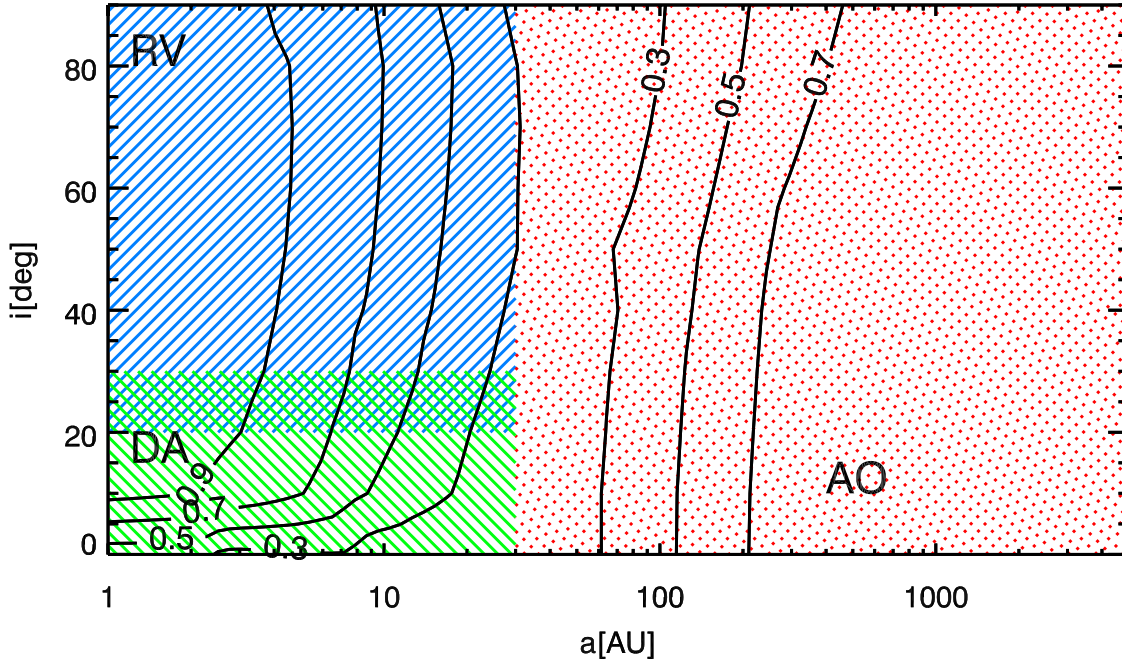


FIG. 2.— Typical completeness contours for 3 techniques used to detect and constrain stellar companions around planet host stars. The radial velocity (RV) technique is sensitive to stellar companions within  $\sim 30$  AU and with small or intermediate mutual inclinations to planet orbital planes (blue hatched region). Note that  $i$  is the angle between the stellar companion orbital plane and the sky plane, so  $i \sim 90^\circ$  implies a small mutual inclination between the stellar companion orbital plane and a transiting planet orbital plane. Dynamical analysis (DA) is sensitive to stellar companions at larger mutual inclinations between the stellar companion orbital plane and a transiting planet orbital plane (green hatched region). The adaptive optics (AO) imaging technique is sensitive to stellar companions at wider orbits (red dotted region). The combination of these 3 techniques contributes to a survey of stellar companions with high completeness.

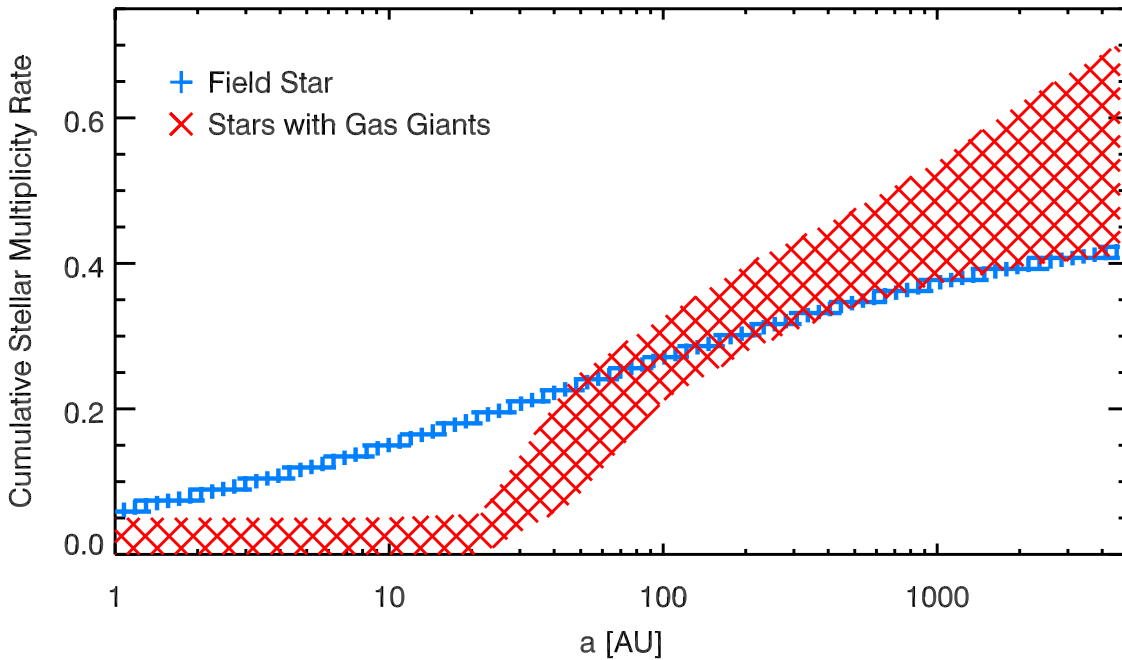


FIG. 3.— Comparison of the cumulative stellar multiplicity rate between field stars in the solar neighborhood (blue) and gas giant planet host stars (red). Hatched regions represent  $1\text{-}\sigma$  uncertainty regions. The stellar multiplicity rate for planet host stars is  $0^{+5}_{-0}\%$  within 20 AU. In comparison, the stellar multiplicity rate is  $18\% \pm 2\%$  for the control sample. The stellar multiplicity rate for planet host star is  $34\% \pm 8\%$  for separations between 20 and 200 AU, which is higher than the control sample at  $12\% \pm 2\%$ . Beyond 200 AU, stellar multiplicity rates are comparable between planet host stars and the control sample

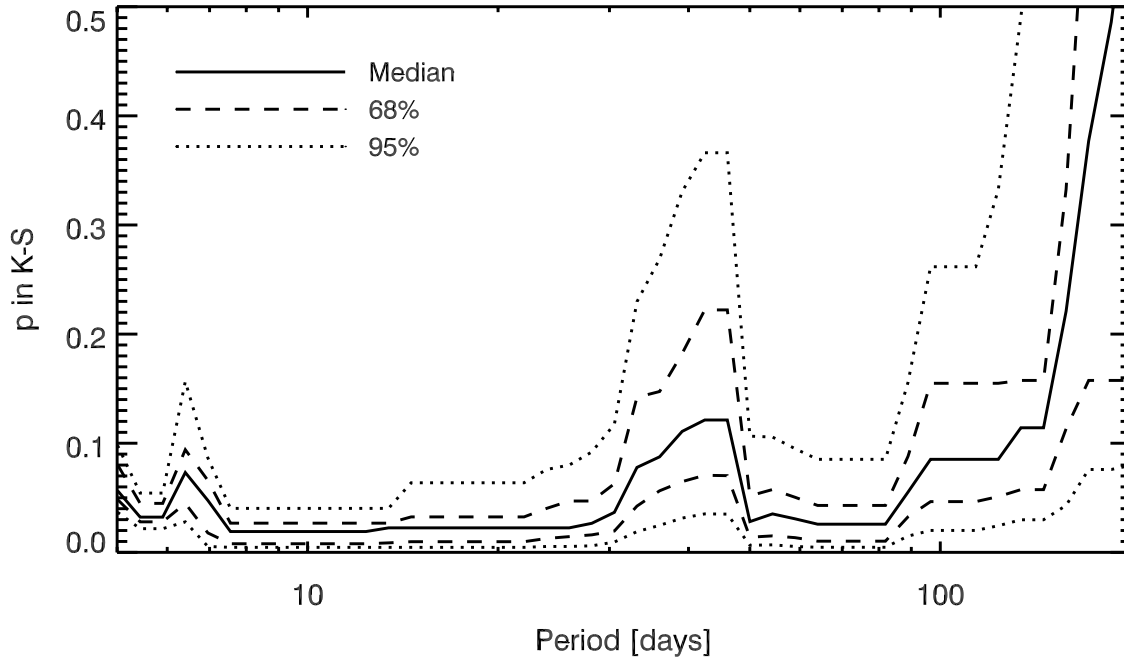


FIG. 4.— Results of K-S tests for the null hypothesis that stars with shorter-period and longer-period gas giant planets have stellar companions with similar distribution of differential magnitude. At each dividing period, we conduct a Monte Carlo simulation and show the median (solid), 68% (dashed) and 95% (dotted) confidence intervals. There may be three populations of gas giant planets whose formation and evolution are influenced differently by their stellar companions. The dividing periods for these populations are  $\sim 10$  and  $\sim 70$  days.

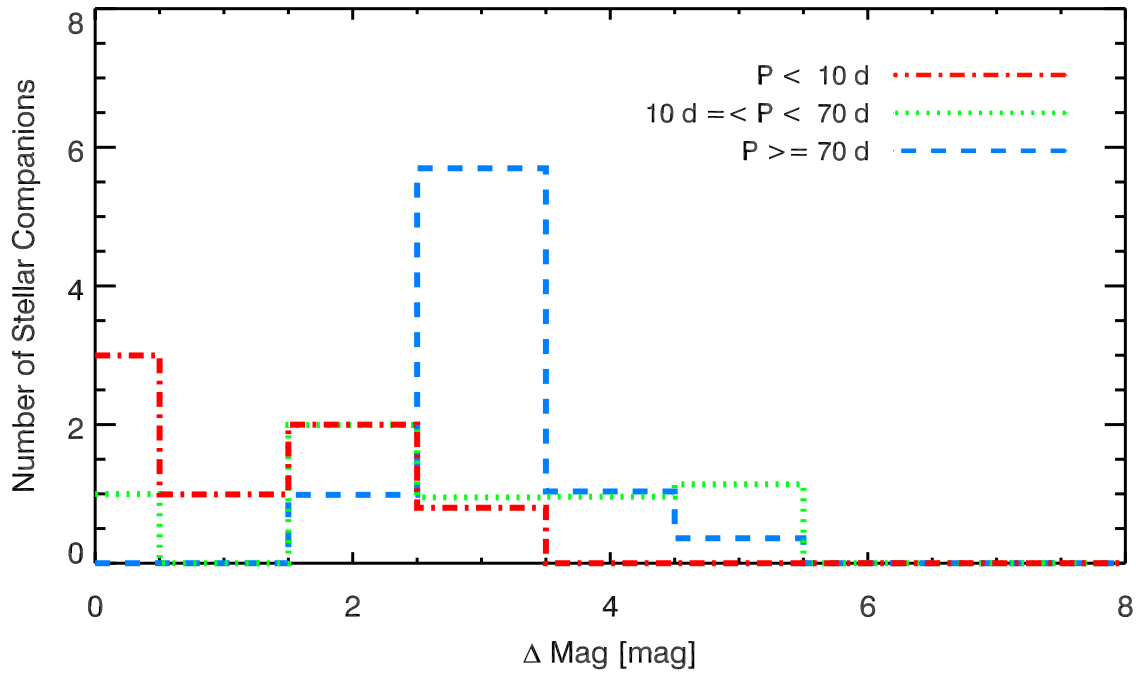


FIG. 5.— The distribution of differential magnitude for stellar companions. For stars with short-period gas giant planets ( $P < 10$  days), stellar companions tend to be bright with small differential magnitudes. For stars with gas giant planets with  $P \geq 70$  days, the differential magnitudes of their stellar companions tend to be fainter than the short-period counterparts. There is a peak at  $\sim 3.0$  mag, but it may be due to a lack of sensitivity for fainter stellar companions.

TABLE 1  
 RV AND AO DATA FOR 97 KOIS

KOI	KIC	KOI							#PL	$R_{PL}$ ( $R_{\oplus}$ )	Period (day)	$T_{start}$ (MJD)	RV
		$\alpha$ (deg)	$\delta$ (deg)	$K_P$ (mag)	$T_{eff}$ (K)	$\log g$ (cgs)	$d$ (pc)	$T_{end}$ (MJD)					
K00001.01	11446443	286.808472	49.316399	11.338	5814.00	4.380	207.0	1	14.40±1.60	2.470613	54216.610352	56208.22753	
K00003.01	10748390	297.709351	48.080853	9.174	4766.00	4.590	38.8	1	4.68±0.18	4.887800	54336.352539	56485.62695	
K00005.01	8554498	289.739716	44.647419	11.665	5861.00	4.190	286.6	2	5.66±0.72	4.780329	54983.515625	56486.43945	
K00010.01	6922244	281.288116	42.451080	13.563	6025.00	4.110	919.7	1	15.90±2.10	3.522499	54983.540039	55781.53418	
K00017.01	10874614	296.837250	48.239944	13.303	5826.00	4.420	494.3	1	11.07±0.54	3.234700	54984.560547	55043.51953	
K00020.01	11804465	286.243439	50.040379	13.438	6011.00	4.230	608.4	1	17.60±2.50	4.437963	55014.412109	55761.32519	
K00022.01	9631995	282.629669	46.323360	13.435	5972.00	4.410	593.4	1	11.27±0.70	7.891450	55014.403320	55792.43847	
K00046.01	10905239	283.255493	48.355232	13.770	5764.00	4.400	604.1	2	4.33±0.37	3.487688			
K00063.01	11554435	289.226166	49.548199	11.582	5721.00	4.470	212.3	1	6.31±0.31	9.434158			
K00094.02	6462863	297.333069	41.891121	12.205	6184.00	4.181	463.6	4	4.22±0.42	10.423707			
K00094.03	6462863	297.333069	41.891121	12.205	6184.00	4.181	463.6	4	6.73±0.67	54.319930			
K00094.01	6462863	297.333069	41.891121	12.205	6184.00	4.181	463.6	4	11.40±1.10	22.343001			
K00097.01	5780885	288.581512	41.089809	12.885	5934.00	4.040	789.7	1	16.10±2.00	4.885489	55106.878906	55115.87109	
K00098.01	10264660	287.708832	47.333050	12.128	6395.00	4.150	446.2	1	10.00±1.40	6.790123	55440.500987	56533.43359	
K00108.02	4914423	288.984558	40.064529	12.287	5975.00	4.330	354.6	2	4.46±0.52	179.601000	55073.468750	56145.49804	
K00119.01	9471974	294.559174	46.062328	12.654	5632.00	4.440	313.0	2	3.90±2.60	49.184310			
K00127.01	8359498	289.607971	44.345421	13.938	5731.00	4.450	617.4	1	10.93±0.47	3.578783			
K00128.01	11359879	296.200592	49.140121	13.758	5786.00	4.420	579.8	1	11.97±0.85	4.942783	55284.481445	55509.07519	
K00131.01	7778437	299.097534	43.497589	13.797	6411.00	4.400	937.3	1	9.00±3.20	5.014233			
K00135.01	9818381	285.240845	46.668251	13.958	6082.00	4.370	810.1	1	10.56±0.46	3.024095	55752.008789	55806.83398	
K00137.01	8644288	298.079437	44.746319	13.549	5385.00	4.430	421.9	3	4.75±0.43	7.641571	55075.508789	56146.48437	
K00137.02	8644288	298.079437	44.746319	13.549	5385.00	4.430	421.9	3	6.01±0.54	14.858940	55075.508789	56146.48437	
K00139.01	8559644	291.653168	44.688271	13.492	5952.00	4.380	612.0	2	7.34±0.66	224.797120			
K00141.01	12105051	288.038300	50.651611	13.687	5425.00	4.500	463.1	1	5.43±0.29	2.624234			
K00152.01	8394721	300.517120	44.381580	13.914	6405.00	4.420	897.1	4	6.10±1.90	52.091100			
K00157.03	6541920	297.115112	41.909142	13.709	5685.00	4.380	514.8	6	4.18±0.76	31.995467	55440.500987	56533.43359	
K00179.02	9663113	297.045410	46.328701	13.955	6081.00	4.420	771.2	2	5.00±1.70	572.397900			
K00244.01	4349452	286.638397	39.487881	10.734	6103.00	4.070	313.5	2	6.51±0.89	12.720365	55366.602539	56519.40820	
K00279.01	12314973	295.486511	51.013500	11.684	6418.00	4.280	268.6	3	5.10±1.60	28.454899			
K00289.02	10386922	282.945648	47.574905	12.747	5812.00	4.458	348.4	2	5.04±0.00	296.637100	56449.400391	56532.29101	
K00318.01	8156120	288.153992	44.068821	12.211	6285.00	4.290	415.8	1	5.19±0.49	38.583360			
K00319.01	8684730	290.117523	44.872940	12.711	5952.00	4.190	421.3	1	7.50±1.10	46.151590			
K00340.01	10616571	297.664673	47.801392	13.057	5811.00	4.400	417.3	1	16.80±1.40	23.673188			
K00344.01	11015108	283.340271	48.549042	13.400	5984.00	4.340	597.5	1	3.80±1.60	39.309240			
K00351.02	11442793	284.433502	49.305161	13.804	6330.00	4.430	870.7	6	6.80±3.00	210.596590			
K00351.01	11442793	284.433502	49.305161	13.804	6330.00	4.430	870.7	6	9.80±4.20	331.643000			
K00366.01	3545478	291.664185	38.619255	11.714	6207.00	4.180	352.1	1	10.60±4.60	75.112019			
K00367.01	4815520	284.472168	39.911812	11.105	5569.00	4.360	153.6	1	4.98±0.71	31.578680			
K00372.01	6471021	299.122437	41.866760	12.391	5872.00	4.487	355.2	1	8.52±0.23	125.630640			
K00375.01	12356617	291.201202	51.144279	13.293	5757.00	4.140	778.2	1	10.40±1.40	988.881118			
K00377.02	3323887	285.573975	38.400902	13.803	5777.00	4.450	619.4	3	8.22±0.59	38.907202	55342.448242	56506.36328	
K00377.01	3323887	285.573975	38.400902	13.803	5777.00	4.450	619.4	3	8.28±0.59	19.273938	55342.448242	56506.36328	
K00633.01	4841374	293.427032	39.942429	13.871	6070.00	4.030	640.1	1	5.80±1.80	161.479000			
K00638.01	5113822	295.559418	40.236271	13.595	5980.00	4.310	575.9	2	3.80±1.20	23.638883			
K00638.02	5113822	295.559418	40.236271	13.595	5980.00	4.310	575.9	2	3.90±1.30	67.093500			
K00672.02	7115785	291.169525	42.640808	13.998	5524.00	4.410	524.6	3	4.03±0.41	41.749990			
K00680.01	7529266	292.287323	43.197281	13.643	6327.00	4.350	786.9	1	8.00±2.40	8.600145			
K00682.01	7619236	295.197998	43.269508	13.916	5592.00	4.250	632.7	1	10.80±1.40	562.142400			
K00683.01	7630229	297.824310	43.258381	13.714	5887.00	4.390	647.6	1	6.00±0.77	278.122200			
K00686.01	7906882	296.840759	43.647121	13.579	5559.00	4.470	494.5	1	11.40±4.40	52.513565			
K00697.01	8878187	289.000885	45.154270	13.684	5779.00	4.050	1315.7	1	4.24±0.75	3.032154			
K00707.03	9458613	289.077545	46.005219	13.988	5904.00	4.030	1236.7	5	4.10±0.36	31.784660			
K00707.02	9458613	289.077545	46.005219	13.988	5904.00	4.030	1236.7	5	4.69±0.41	41.027950			
K00707.01	9458613	289.077545	46.005219	13.988	5904.00	4.030	1236.7	5	5.50±0.48	21.775754			
K00716.01	9846348	297.492157	46.694519	13.754	6115.00	4.490	713.2	1	6.80±3.20	26.893084			
K01162.01	10528068	288.868225	47.759430	12.783	6138.00	4.280	490.7	1	4.40±2.30	158.692400			
K01206.01	3756801	293.954590	38.899971	13.642	5754.00	4.110	826.9	1	6.20±1.90	422.917678			
K01274.01	8800954	283.256805	45.087780	13.354	5310.00	4.550	356.9	1	4.73±0.28	704.962626			
K01311.01	10713616	283.532959	48.094261	13.498	6188.00	4.200	648.2	1	4.20±1.70	83.577520			
K01335.01	4155328	291.020142	39.220680	13.968	6222.00	4.040	1385.0	1	8.60±2.70	127.832900			
K01353.02	7303287	297.465332	42.882839	13.956	6260.00	4.080	1094.5	2	3.80±1.10	34.543630			
K01353.01	7303287	297.465332	42.882839	13.956	6260.00	4.080	1094.5	2	18.60±5.30	125.865460			
K01375.01	6766634	288.320435	42.261414	13.709	6169.00	4.358	594.0	1	6.78±0.00	321.213900			
K01411.01	9425139	298.995087	45.909512	13.377	5753.00	4.410	502.0	1	7.05±0.84	305.056500			
K01431.01	11075279	287.022278	48.681938	13.460	5649.00	4.460	486.8	1	8.45±0.48	345.161300	56472.390625	56532.50195	
K01439.01	11027624	290.851776	48.521339	12.849	5930.00	4.090	719.2	1	7.80±1.10	394.610700	55075.273438	56531.31250	
K01474.01	12365184	295.417877	51.184761	13.005	6293.00	4.270	552.0	1	9.30±1.20	69.732970			
K01478.01	12403119	288.848633	51.209049	12.450	5493.00	4.417	288.4	1	5.26±0.35	76.133540			
K01645.01	11045383	298.210938	48.559158	13.418	5197.00	4.530	379.9	1	10.31±3.10	41.166759			
K01658.01	4570949	294.192108	39.618999	13.308	6422.00	4.320	750.6	1	12.35±0.67	1.544930			
K01684.01	6048024	293.534485	41.329899	12.849	6387.00	4.430	616.1	1	7.30±2.60	62.815570			
K01779.02	9909735	298.482819	46.793621	13.297	5812.00	4.140	586.3	2	5.00±1.70	11.815018			
K01779.01	9909735	298.482819	46.793621	13.297	5812.00	4.140	586.3	2	5.80±1.90	4.662723			
K01783.02	10005758	289.341431	46.988239	13.929	6235.00	4.460	845.5	2	5.20±1.90	284.042300			

TABLE 2  
RV AND AO DATA FOR 97 KOIS

KOI	KIC	KOI							#PL	$R_{PL}$ ( $R_{\oplus}$ )	Period (day)	$T_{start}$ (MJD)	RV $T_{end}$ (MJD)	#RV
		$\alpha$ (deg)	$\delta$ (deg)	$K_P$ (mag)	$T_{eff}$ (K)	$\log g$ (cgs)	$d$ (pc)							
K01783.01	10005758	289.341431	46.988239	13.929	6235.00	4.460	845.5	2	8.50±3.10	134.479720				
K01784.01	10158418	297.646057	47.167488	13.592	5853.00	4.540	574.0	1	5.20±3.00	5.007410				
K01792.01	8552719	288.971649	44.624531	12.160	5689.00	4.440	300.1	3	4.61±0.27	88.407030				
K01800.01	11017901	285.268585	48.560009	12.394	5600.00	4.430	307.9	1	6.20±2.10	7.794300				
K01805.02	4644952	288.811951	39.770660	13.828	5708.00	4.080	789.5	3	4.30±1.20	31.782260				
K01805.01	4644952	288.811951	39.770660	13.828	5708.00	4.080	789.5	3	5.60±1.50	6.941344				
K01808.01	7761918	294.743317	43.461208	12.487	6278.00	4.350	424.4	1	4.00±1.60	89.192840				
K01812.01	6279974	290.126526	41.601082	13.742	6285.00	4.420	778.7	1	4.80±1.80	0.805263				
K01825.01	5375194	295.300079	40.556591	13.895	5545.00	4.060	904.3	1	4.20±1.10	13.522604				
K02672.01	11253827	296.132812	48.977402	11.921	5565.00	4.330	236.0	2	5.30±2.10	88.516580				
K02674.01	8022489	289.651245	43.824421	13.349	5973.00	4.260	501.1	3	7.30±2.60	197.510340				
K02677.01	9958387	294.757690	46.831120	13.460	6409.00	4.340	694.7	1	6.50±1.00	237.788200				
K03444.02	5384713	297.429199	40.561909	13.693	3842.00	4.664	122.4	4	5.74±3.20	60.326632				
K03663.01	12735740	289.763611	51.962601	12.620	6007.00	4.340	394.8	1	11.29±0.03	282.525503				
K03678.01	4150804	289.791595	39.285328	12.888	5650.00	4.313	413.8	1	9.12±0.04	160.885644				
K03787.01	7813039	288.439117	43.505249	13.891	5993.00	4.355	741.5	1	9.17±1.10	141.733971				
K03791.02	5437945	288.474854	40.651360	13.771	6340.00	4.163	932.2	2	5.65±0.21	220.130023				
K03791.01	5437945	288.474854	40.651360	13.771	6340.00	4.163	932.2	2	7.21±0.11	440.785197				
K03811.01	4638237	286.153107	39.714901	13.906	5551.00	4.518	505.5	1	6.98±0.99	290.140253				
K03823.01	4820550	286.771454	39.983822	13.922	5817.00	4.544	663.9	1	5.54±0.08	202.117797				
K03875.01	11911561	290.149139	50.239178	13.579	6022.00	4.027	660.4	1	4.73±0.70	8.870420				
K03907.01	7137213	296.997803	42.653320	12.642	6498.00	4.081	610.0	1	4.05±0.88	28.643425				
K05515.01	8429817	291.452271	44.431751	13.952	6247.00	4.255	806.9	1	8.88±1.50	6.263490				

TABLE 3  
VISUAL COMPANION DETECTIONS WITH AO DATA.

KOI	$\Delta$ Mag (mag)	Separation		Distance		Detection Significance ( $\sigma$ )	PA (deg)	Association Probability	ref.
		(arcsec)	(AU)	Primary (pc)	Secondary (pc)				
K00001	4.0 ( <i>i</i> )	1.13	...	...	259.0 <sup>+1915.3</sup> <sub>-231.2</sub>	...	135.0	...	L14
	4.3 ( <i>r</i> )	1.11	...	...	...	...	135.5	0.98	H14
	3.3 ( <i>z</i> )	1.11	...	...	...	...	136.3	0.99	H14
	2.8 (J)	1.12	232.6	207.0 <sup>+22.4</sup> <sub>-29.2</sub>	...	233.5	136.2	1.00	this work
	2.5 (H)	1.11	230.5	207.0 <sup>+22.4</sup> <sub>-29.2</sub>	...	383.6	136.3	1.00	this work
	2.4 (K)	1.12	230.9	207.0 <sup>+22.4</sup> <sub>-29.2</sub>	...	68.5	136.5	1.00	this work
K00005	2.3 (K)	0.14	40.3	286.6 <sup>+71.1</sup> <sub>-15.8</sub>	...	19.2	308.9	1.00	CFOP
<b>K00010*</b>	7.7 (J)	3.04	2795.9	919.7 <sup>+96.5</sup> <sub>-126.8</sub>	...	...	94.3	0.00	A12
K00010	6.2 (J)	3.74	3439.7	919.7 <sup>+96.5</sup> <sub>-126.8</sub>	...	14.9	89.3	0.15	A12
K00017	3.8 (J)	4.01	1982.1	494.3 <sup>+42.6</sup> <sub>-65.0</sub>	...	132.6	39.9	0.75	A12
<b>K00020*</b>	7.9 (J)	5.04	3066.3	608.4 <sup>+135.9</sup> <sub>-20.1</sub>	...	...	139.6	0.00	A12
K00097	4.0 (J)	1.90	1500.4	789.7 <sup>+56.9</sup> <sub>-119.2</sub>	3847.0 <sup>+2111.4</sup> <sub>-1270.0</sub>	49.8	105.1	0.90	A12
	4.0 (K)	1.91	1508.3	789.7 <sup>+56.9</sup> <sub>-119.2</sub>	...	81.0	105.1	0.89	A12
K00098	0.1 ( <i>i</i> )	0.29	...	...	707.4 <sup>+1094.4</sup> <sub>-533.0</sub>	...	140.0	...	L14
	0.5 ( <i>r</i> )	0.29	...	...	...	...	140.0	1.00	H14
	0.7 ( <i>z</i> )	0.29	...	...	...	...	140.3	1.00	H14
	0.3 (J)	0.27	120.5	446.2 <sup>+109.2</sup> <sub>-29.0</sub>	...	...	143.7	1.00	A12
	0.4 (K)	0.28	124.9	446.2 <sup>+109.2</sup> <sub>-29.0</sub>	...	15.7	143.5	1.00	A12
K00098	6.2 (J)	5.60	2498.7	446.2 <sup>+109.2</sup> <sub>-29.0</sub>	2604.5 <sup>+344.9</sup> <sub>-930.6</sub>	20.8	306.3	0.13	A12
	5.6 (K)	5.59	2494.3	446.2 <sup>+109.2</sup> <sub>-29.0</sub>	...	12.0	306.1	0.16	A12
K00098	7.2 (J)	6.20	2766.1	446.2 <sup>+109.2</sup> <sub>-29.0</sub>	422.4 <sup>+609.7</sup> <sub>-139.4</sub>	9.5	237.9	0.00	this work
	6.3 (K)	6.21	2769.5	446.2 <sup>+109.2</sup> <sub>-29.0</sub>	...	5.1	237.9	0.24	this work
<b>K00108*</b>	7.2 (J)	2.44	865.2	354.6 <sup>+45.4</sup> <sub>-39.2</sub>	...	...	74.9	0.35	A12
<b>K00108*</b>	7.2 (J)	4.87	1726.9	354.6 <sup>+45.4</sup> <sub>-39.2</sub>	...	...	112.4	0.00	A12
K00119	0.9 ( <i>i</i> )	1.05	...	...	216.1 <sup>+302.3</sup> <sub>-77.2</sub>	...	118.0	...	L14
	0.2 (J)	1.05	327.5	313.0 <sup>+106.8</sup> <sub>-62.2</sub>	...	116.2	118.4	0.60	this work
	0.2 (K)	1.05	327.5	313.0 <sup>+106.8</sup> <sub>-62.2</sub>	...	96.7	118.4	1.00	this work
K00137	4.1 (J)	5.59	2359.2	421.9 <sup>+45.0</sup> <sub>-54.0</sub>	...	116.7	349.8	0.57	A12
<b>K00137*</b>	7.9 (J)	4.80	2025.1	421.9 <sup>+45.0</sup> <sub>-54.0</sub>	...	...	340.5	0.00	A12
<b>K00137*</b>	7.5 (J)	4.98	2101.1	421.9 <sup>+45.0</sup> <sub>-54.0</sub>	...	...	136.3	0.00	A12
K00141	1.4 ( <i>i</i> )	1.10	...	...	957.8 <sup>+1256.9</sup> <sub>-339.4</sub>	...	11.0	...	L14
	1.2 (J)	1.06	490.9	463.1 <sup>+32.7</sup> <sub>-63.3</sub>	...	192.1	13.9	0.99	A12
	1.4 (K)	1.06	490.9	463.1 <sup>+32.7</sup> <sub>-63.3</sub>	...	242.4	13.5	0.99	A12
K00152	5.7 (K)	2.49	2230.1	897.1 <sup>+162.0</sup> <sub>-162.4</sub>	...	6.0	29.5	0.23	this work
K00157	4.4 (K)	1.36	698.7	514.8 <sup>+115.5</sup> <sub>-93.5</sub>	...	6.0	179.9	0.94	this work
K00157	4.7 (K)	4.09	2104.3	514.8 <sup>+115.5</sup> <sub>-93.5</sub>	...	7.7	238.0	0.35	this work
K00279	3.5 ( <i>r</i> )	0.92	...	...	457.0 <sup>+137.2</sup> <sub>-53.4</sub>	...	246.6	0.99	H14
	3.1 ( <i>z</i> )	0.92	...	...	...	...	247.2	0.99	H14
	2.3 (K)	0.93	250.4	268.6 <sup>+187.6</sup> <sub>-46.3</sub>	...	111.8	246.9	1.00	CFOP
K00340	5.4 (K)	5.34	2227.7	417.3 <sup>+49.8</sup> <sub>-46.5</sub>	...	6.0	57.6	0.10	this work
K00344	3.5 (K)	4.13	2470.2	597.5 <sup>+290.0</sup> <sub>-126.2</sub>	...	45.9	178.9	0.68	this work
K00344	5.2 (K)	3.55	2123.6	597.5 <sup>+290.0</sup> <sub>-126.2</sub>	...	9.7	210.6	0.34	this work
K00366	6.5 (K)	7.00	2464.4	352.1 <sup>+468.6</sup> <sub>-91.7</sub>	...	5.6	70.1	0.02	this work
<b>K00372*</b>	8.6 (K)	2.49	884.4	355.2 <sup>+12.2</sup> <sub>-54.0</sub>	...	...	157.8	0.00	A12
<b>K00372*</b>	8.0 (K)	3.56	1264.5	355.2 <sup>+12.2</sup> <sub>-54.0</sub>	...	...	56.9	0.00	A12
<b>K00372*</b>	8.2 (K)	4.99	1772.4	355.2 <sup>+12.2</sup> <sub>-54.0</sub>	...	...	170.7	0.00	A12
<b>K00372*</b>	4.0 (K)	5.94	2109.9	355.2 <sup>+12.2</sup> <sub>-54.0</sub>	...	...	32.7	0.64	A12
K00375	3.3 (K)	5.47	4254.0	778.2 <sup>+64.2</sup> <sub>-139.5</sub>	...	25.4	157.0	0.64	this work
K00375	4.6 (K)	3.19	2486.2	778.2 <sup>+64.2</sup> <sub>-139.5</sub>	...	5.9	305.5	0.56	this work
K00377	4.5 (J)	5.90	3654.5	619.4 <sup>+54.5</sup> <sub>-102.7</sub>	2639.5 <sup>+578.1</sup> <sub>-308.6</sub>	37.5	91.7	0.31	A12
	4.2 (K)	5.89	3648.3	619.4 <sup>+54.5</sup> <sub>-102.7</sub>	...	101.0	91.7	0.34	A12
<b>K00377*</b>	6.8 (J)	2.79	1728.1	619.4 <sup>+54.5</sup> <sub>-102.7</sub>	9717.3 <sup>+2629.4</sup> <sub>-1745.8</sub>	...	37.9	0.10	A12
K00377	6.6 (K)	2.79	1728.1	619.4 <sup>+54.5</sup> <sub>-102.7</sub>	...	10.9	37.8	0.02	A12
K00633	3.9 (K)	0.67	432.0	640.1 <sup>+612.4</sup> <sub>-71.0</sub>	...	18.2	18.4	0.97	this work
K00683	4.0 (K)	3.42	2214.4	647.6 <sup>+69.5</sup> <sub>-92.2</sub>	...	8.2	268.9	0.32	this work

NOTE. — \*: stellar companions that are not detected by our detection pipeline. References: A12 - Adams et al. (2012); D14 - Dressing et al. (2014); H14 - Horch et al. (2014); L14 - Law et al. (2014); LB14 - Lillo-Box et al. (2014).

TABLE 4  
VISUAL COMPANION DETECTIONS WITH AO DATA.

KOI	$\Delta$ Mag (mag)	Separation		Distance		Detection Significance ( $\sigma$ )	PA (deg)	Association Probability	ref.
		(arcsec)	(AU)	Primary (pc)	Secondary (pc)				
K00697	0.0 (J)	0.66	868.4	$1315.7^{+209.8}_{-727.9}$	$671.3^{+1881.0}_{-424.2}$	235.5	55.3	1.00	this work
	0.0 (H)	0.66	868.4	$1315.7^{+209.8}_{-727.9}$	...	257.4	55.2	1.00	this work
	0.0 (K)	0.66	868.4	$1315.7^{+209.8}_{-727.9}$	...	257.1	55.7	1.00	this work
K01274	3.8 (i)	1.10	...	...	$412.2^{+81.1}_{-96.6}$	...	241.0	...	L14
	2.4 (K)	1.09	389.0	$356.9^{+34.1}_{-55.8}$	...	9.0	242.7	0.99	this work
K01335	4.6 (K)	4.51	6244.0	$1385.0^{+209.1}_{-635.9}$	...	17.3	358.1	0.26	this work
K01353	5.4 (K)	3.17	3466.8	$1094.5^{+403.6}_{-410.2}$	...	7.0	63.3	0.19	this work
K01353	5.9 (K)	5.65	6186.2	$1094.5^{+403.6}_{-410.2}$	...	5.0	97.9	0.00	this work
K01375	4.4 (i)	0.77	...	...	$1907.7^{+12041.7}_{-557.2}$	...	269.0	...	L14
	3.8 (J)	0.80	473.2	$594.0^{+675.6}_{-94.2}$	...	23.6	270.0	0.97	this work
	3.6 (H)	0.79	467.5	$594.0^{+675.6}_{-94.2}$	...	48.7	269.5	0.98	this work
	3.6 (K)	0.79	470.3	$594.0^{+675.6}_{-94.2}$	...	26.4	269.9	0.98	this work
K01411	5.3 (K)	3.79	1904.2	$502.0^{+43.3}_{-62.1}$	...	7.1	147.4	0.14	this work
K01463	6.4 (K)	6.11	2122.1	$347.5^{+358.6}_{-73.1}$	...	5.4	233.7	0.03	this work
K01784	0.9 (J)	0.28	160.7	$574.0^{+94.1}_{-117.7}$	$575.8^{+2878.2}_{-445.1}$	16.8	288.4	1.00	this work
	0.8 (H)	0.28	160.7	$574.0^{+94.1}_{-117.7}$	...	10.6	286.6	1.00	this work
	0.7 (K)	0.28	160.7	$574.0^{+94.1}_{-117.7}$	...	6.6	291.0	1.00	this work
K01808	3.3 (K)	4.68	1986.0	$424.4^{+177.3}_{-70.8}$	...	93.4	163.1	0.74	this work
K01812	4.3 (i)	2.37	...	...	$2173.3^{+254.0}_{-182.1}$	...	...	...	LB14
	3.6 (K)	2.37	1844.2	$778.7^{+168.5}_{-139.5}$	...	21.6	297.9	0.82	this work
K01825	4.4 (K)	5.56	5025.4	$904.3^{+133.3}_{-388.6}$	...	25.9	295.3	0.20	this work
K02672	3.5 (K)	0.69	163.6	$236.0^{+126.7}_{-46.5}$	...	44.2	302.9	0.99	CFOP
K02672	5.9 (K)	4.54	...	...	...	...	308.0	...	D14
	6.0 (K)	4.61	1088.0	$236.0^{+126.7}_{-46.5}$	...	10.9	310.4	0.23	this work
K03444	2.8 (i)	1.08	...	...	$179.4^{+372.5}_{-128.1}$	...	9.6	...	LB14
	2.6 (z)	1.08	...	...	...	...	9.6	0.99	LB14
	2.2 (J)	1.08	132.2	$122.4^{+24.9}_{-27.1}$	...	12.3	9.5	1.00	this work
	2.4 (K)	1.08	132.2	$122.4^{+24.9}_{-27.1}$	...	40.7	9.5	1.00	this work
K03444	4.5 (i)	3.58	...	...	$1878.9^{+3063.4}_{-812.6}$	...	264.4	...	LB14
	4.7 (z)	3.58	...	...	...	...	264.4	0.71	LB14
	5.0 (J)	3.63	443.8	$122.4^{+24.9}_{-27.1}$	...	11.5	264.8	0.63	this work
	5.3 (K)	3.57	436.7	$122.4^{+24.9}_{-27.1}$	...	26.9	264.8	0.58	this work
K03678	3.3 (K)	2.61	1081.7	$413.8^{+200.9}_{-57.5}$	...	33.9	169.6	0.85	this work
K03787	5.1 (K)	6.96	5162.8	$741.5^{+328.6}_{-132.0}$	...	9.2	254.9	0.12	this work
K03823	5.6 (K)	2.33	1546.0	$663.9^{+233.3}_{-87.5}$	...	10.0	58.0	0.36	this work
K03823	5.1 (K)	5.06	3357.5	$663.9^{+233.3}_{-87.5}$	...	14.9	239.4	0.12	this work
K03907	2.5 (J)	2.77	1689.5	$610.0^{+375.2}_{-135.7}$	$588.4^{+3714.2}_{-521.8}$	55.0	74.2	0.95	this work
	2.2 (H)	2.75	1674.6	$610.0^{+375.2}_{-135.7}$	...	140.3	74.3	0.94	this work
	2.1 (K)	2.76	1681.5	$610.0^{+375.2}_{-135.7}$	...	97.2	74.1	0.96	this work
K03907	4.3 (J)	1.59	968.7	$610.0^{+375.2}_{-135.7}$	$99.5^{+1267.3}_{-29.0}$	10.6	162.3	0.93	this work
	3.7 (H)	1.57	958.0	$610.0^{+375.2}_{-135.7}$	...	41.0	163.4	0.95	this work
	3.5 (K)	1.57	955.2	$610.0^{+375.2}_{-135.7}$	...	27.9	163.1	0.96	this work
K05515	4.1 (J)	2.36	1907.5	$806.9^{+288.9}_{-138.7}$	$2059.3^{+13563.5}_{-1925.1}$	24.3	297.9	0.79	this work
	3.6 (H)	2.36	1907.4	$806.9^{+288.9}_{-138.7}$	...	44.3	297.7	0.82	this work
	3.7 (K)	2.37	1915.9	$806.9^{+288.9}_{-138.7}$	...	23.2	297.7	0.80	this work
K05515	5.4 (J)	2.67	2158.2	$806.9^{+288.9}_{-138.7}$	$4443.6^{+25325.9}_{-4134.8}$	9.1	114.2	0.47	this work
	5.1 (H)	2.68	2159.2	$806.9^{+288.9}_{-138.7}$	...	12.9	114.4	0.45	this work
	5.1 (K)	2.67	2155.6	$806.9^{+288.9}_{-138.7}$	...	6.4	114.5	0.41	this work

NOTE. — \*: stellar companions that are not detected by our detection pipeline. References: A12 - Adams et al. (2012); D14 - Dressing et al. (2014); H14 - Horch et al. (2014); L14 - Law et al. (2014); LB14 - Lillo-Box et al. (2014).